

8-2018

A cancer-targeted gold nanoparticle-based MRI contrast agent.

Nagwa El-Baz
University of Louisville

Follow this and additional works at: <https://ir.library.louisville.edu/etd>

 Part of the [Nanomedicine Commons](#)

Recommended Citation

El-Baz, Nagwa, "A cancer-targeted gold nanoparticle-based MRI contrast agent." (2018). *Electronic Theses and Dissertations*. Paper 3018.
<https://doi.org/10.18297/etd/3018>

This Master's Thesis is brought to you for free and open access by ThinkIR: The University of Louisville's Institutional Repository. It has been accepted for inclusion in Electronic Theses and Dissertations by an authorized administrator of ThinkIR: The University of Louisville's Institutional Repository. This title appears here courtesy of the author, who has retained all other copyrights. For more information, please contact thinkir@louisville.edu.

A CANCER-TARGETED GOLD NANOPARTICLE-BASED MRI CONTRAST
AGENT

By

Nagwa El-Baz

B.S. Pharmacy School, Mansoura University, 2001

A Thesis

Submitted to the Faculty of the School of Medicine of the University of Louisville in

Partial Fulfillment of the Requirements for the Degree of

Master of Science in Pharmacology and Toxicology

Department of Pharmacology and Toxicology

University of Louisville

Louisville, Kentucky

August 2018

A CANCER-TARGETED GOLD NANOPARTICLE-BASED MRI CONTRAST
AGENT

By

Nagwa El-Baz

B.S. Pharmacy School, Mansoura University, 2001

A Thesis Approved on July 5, 2018

By the following Thesis Committee

Martin O'Toole, Ph.D.

Tariq Malik, Ph.D.

Geoffrey Clark, Ph.D.

Hermann Frieboes, Ph.D.

Jill Steinbach-Rankins, Ph.D.

DEDICATION

To my mother, my husband, my kids, my sister and brothers, I couldn't have done this without your affections, support, and love. You mean the world to me.

ACKNOWLEDGMENTS

I would like to express the deepest appreciation to my primary mentor Dr. O'Toole for providing guidance, supervision, and insight throughout the research project.

I would like to express my deepest thanks to Dr. Malik for his guidance and help in cells and animals' studies.

I would like to thank all the committee members

I would like to thank Dr. Keynton for his support.

I would like to thank Dr. Chauhan, Kurtis James, and Danial Malik for their help and I would like to thank all and the members of Dr. O'Toole's lab.

ABSTRACT

A CANCER-TARGETED GOLD NANOPARTICLE-BASED MRI CONTRAST AGENT

Nagwa El-Baz

July 5, 2018

In oncology, imaging plays a major role in terms of early detection and treatment of most types of cancer. Magnetic resonance imaging (MRI) is mostly used for cancer diagnosis due to its excellent contrast resolution. However, MRI for cancer diagnosis is somewhat limited by its sensitivity. In this thesis, we assessed the ability of theranostic platform consisting of gold nanoparticles functionalized with a cancer targeting aptamer; AS1411 and gadolinium chelate (Dotarem thiol derivative; Gd (III)-DO3A) as a MRI contrast agent to target malignant tumors by enhancing the MRI contrast of the detected tumor. The proposed technology is a novel injectable contrast agent for detection and monitoring of malignancies by MRI. The gold nanoparticle core (GNPs) enhances the pharmacokinetic properties of the proposed contrast agent, increases its potency, and provides a good way to co-localize the aptamer with the contrast agent. AS1411 is anti-nucleolin aptamer that binds to nucleolin protein, which is highly expressed in cancer cells, leading to selective accumulation in cancers cells. The ability of the proposed contrast agent to target cancer cells and enhance MRI contrast was assessed using MDA-MB-231

triple negative breast cells and MCF-10 human mammary epithelial cells. Moreover we assessed the biodistribution and toxicity of the proposed contrast agent in vivo.

The results presented in this thesis demonstrate the superiority of the proposed contrast agent with respect to the current commercial contrast agents (e.g., MultiHance).

TABLE OF CONTENTS

DEDICATIONS	iii
ACKNOWLEDGMENTS	iv
ABSTRACT	v
LIST OF FIGURES	viii
CHAPTER 1: INTRODUCTION	1
CHAPTER 2: MATERIALS AND METHODS	9
CHAPTER 3: RESULTS AND DISCUSSION	22
CHAPTER 4: CONCLUSION	43
REFERENCES	46
CURRICULUM VITAE	49

LIST OF FIGURES

1	Estimated Numbers of Cancer Cases for 2018 in the USA, excluding basal cell and squamous cell skin cancers and in situ carcinomas except urinary bladder.	2
2	GNP functionalized with Gd (III) DO3A-SH and AS1411.	7
3	Gd ion is chelating to DO3A with thiol group.	8
4	Illustration of the proposed relaxivity calculation.	18
5	An illustration of color map generated of relaxivity enhancement. Red color means 100% improvement in the relaxivity as demonstrated in the color coded bar.	18
6	TEM image and particle size histogram for GNP- <i>Gd-DO3A-SH-AS1411</i> (n=500).	23
7	TEM image and particle size histogram for GNP- <i>Gd-DO3A-SH-CRO</i> (n=500).	23
8	TEM image and particle size histogram for GNP- <i>Gd-DO3A-SH-CTR</i> (n=500).	24
9	Darkfield (Left) and Fluorescence (Right) characterization of OliGreen tagged GNP-Gd(III) DO3A-SH-AS1411(Top), GNP-Gd(III)-DO3A-SH (middle) and non-OliGreen tagged GNP-AS1411 (Bottom).	25

10	Energy Dispersive X-Ray Spectrum of GNP Gd(III) DO3A-SH AS1411.	27
11	Energy Dispersive X-Ray Spectrum of GNP- <i>Gd(III)DO3A-SH-CRO</i> .	27
12	Energy Dispersive X-Ray Spectrum of GNP- <i>Gd(III)DO3A-SH-CTR</i>	28
13	T1-Weighted contrast enhancement comparison for GNP <i>Gd(III)DO3A-SH</i> Oligonucleotide.	30
14	T1-Weighted contrast enhancement comparison for GNP <i>Gd(III)DO3A-SH</i> Oligonucleotide in MCF-10A cell line using T1-Weighted image analysis algorithm after 24 hours.	32
15	T1-Weighted contrast enhancement comparison for GNP <i>Gd(III)DO3A-SH</i> Oligonucleotides in MCF-10A cell line using T1-Weighted image analysis algorithm after 48 hours.	32
16	T1-Weighted contrast enhancement comparison for GNP <i>Gd(III)DO3A-SH</i> Oligonucleotide in MCF-10A cell line using T1-Weighted image analysis algorithm after 72 hours.	33
17	T1-Weighted contrast enhancement comparison for GNP <i>Gd(III)DO3A-SH</i> Oligonucleotide in MCF-10A cell line using T1-Weighted image analysis algorithm after 96 hours.	33
18	T1-Weighted contrast enhancement comparison for GNP <i>Gd(III)DO3A-SH</i> Oligonucleotide in MDA-MB-231 cell line using T1-Weighted image analysis algorithm after 24 hours.	34
19	T1-Weighted contrast enhancement comparison for GNP <i>Gd(III)DO3A-SH</i> Oligonucleotide in MDA-MB-231 cell line using T1-Weighted image analysis	34

	algorithm after 48 hours.	
20	T1-Weighted contrast enhancement comparison for GNP <i>Gd(III)DO3A-SH</i> Oligonucleotide in MDA-MB-231 cell line using T1-Weighted image analysis algorithm after 72 hours.	35
21	T1-Weighted contrast enhancement comparison for GNP <i>Gd(III)DO3A-SH</i> Oligonucleotide in MDA-MB-231 cell line using T1-Weighted image analysis algorithm after 96 hours.	35
22	Uptake and biodistribution of gold in different body organs.	36
23	BUN post-treatment blood concentrations of 5 treatment groups.	38
24	CREA post-treatment blood concentrations of 5 treatment groups.	38
25	ALT post-treatment blood concentrations of 5 treatment groups.	38
26	ALKP post-treatment blood concentrations of 5 treatment groups.	39
27	TBIL post-treatment blood concentrations of 5 treatment groups.	39

CHAPTER 1. INTRODUCTION

1.1. Current Technology for Cancer Diagnosis:

Cancer is a major public health problem worldwide and the second leading cause of death in the United States [1]. Cancer is a group of diseases that can be characterized by uncontrolled growth of abnormal cells. If the cell growth is not controlled, it can result in metastasis of the cancer, and eventually, death. In 2018, about 1.7 million new cancer cases are expected to be diagnosed [2]. Moreover, about 609,640 Americans are expected to die of cancer in 2018 (see Figure 1) [2]. As reported by the American Cancer Society, in 2015, the cancer mortality rate had dropped 26% from its peak in 1991. This decline translated into about 2.4 million deaths avoided during this time period [2]. One of the main reasons for this drop is the improvement in early detection and treatment of most types of cancer. Nowadays, medical imaging plays an important role in diagnosis, staging, monitoring therapeutic response, and treatment planning for almost all cancer types. Each year in USA, more than 71 million Computed Tomography (CT) and 33 million Magnetic Resonance Imaging (MRI) scans are performed for the purpose of detection of primary or metastatic malignant tumors [3]. CT, MRI, and Positron Emission Tomography (PET) are the three major imaging modalities in clinical radiology that are used in cancer diagnosis and treatment.

CT scans combine a series of X-ray images which are taken from different angles and uses computer processing to create cross-sectional images of the interested body organ. CT is the most commonly used modality because it is fast and has widespread availability. CT images provide high resolution of the organ of interest, which can be used to extract all the anatomical features of any detected tumors. Unfortunately, the sensitivity and specificity of diagnosing malignant tumors based only on the anatomical features are low, which makes it unacceptable in the clinical setting. Moreover, some CT intravenous contrast agents are contraindicated with some patients with renal problems. Finally, CT has a limited ability in detected the tumors that may exist in the soft tissues (e.g., brain, liver, etc.)

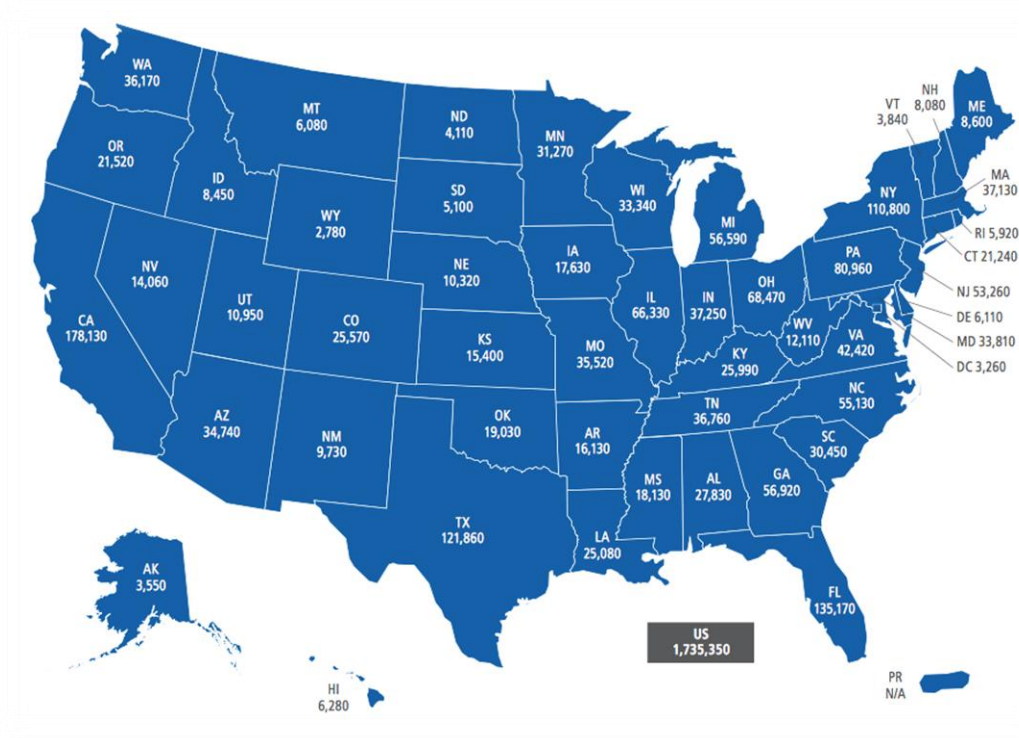


Figure 1: Estimated Numbers of Cancer Cases for 2018 in the USA, excluding basal cell and squamous cell skin cancers and in situ carcinomas except urinary bladder [2].

MRI, also known as nuclear magnetic resonance imaging, is a scanning technique for creating three dimensional detailed images of the regions of interest. To perform an MRI scan, the person is positioned within an MRI scanner that forms a strong magnetic field (that forces the magnetic moment of protons in the body tissues to be aligned with the magnetic field). Then, a radiofrequency pulse is applied which disrupts the protons and forces them to rotate 90 or 180 degrees against the pull of magnetic field. When the radiofrequency pulse is turned off the protons rotate to realign again with the magnetic field, releasing electromagnetic energy. MRI scanners detect the released electromagnetic energy as well the time taken for protons to relax or realign with the magnetic field. These two factors are different depending on the environment of the protons. Technicians can differentiate between different body tissues based on these factors. T1-weighted (spin-lattice) and T2-weighted (spin-spin) are the basic two MRI image types. A T1-weighted image is useful for assessing the cerebral cortex, identifying fatty tissue, characterizing focal liver lesions and in general for obtaining morphological and anatomical information, as well as for post-contrast imaging. A T2-weighted image is useful for detecting edema and inflammation, revealing white matter lesions and assessing zonal anatomy in the prostate and uterus. The main advantage of MRI scans is its ability to detect tumors/lesions in the soft tissues at an early stage [4]. However, MRI sensitivity and specificity for diagnosing malignant tumors is low.

PET is a nuclear medicine functional imaging technique that is used to observe metabolic processes in the body. PET is both a clinical and research tool. PET relies on cancer-selective uptake of radiolabeled sugars and provides better information for malignant status for some (but not all) tumor types; however, its use is limited by its

expense and the necessity for short-lived radiopharmaceuticals that require a synchrotron source. Also, its sensitivity and resolution for diagnosing tumors is low compared with CT and MRI. On the other hand, the main advantage of PET is it has high specificity of tumor diagnosis.

1.2. Current Imaging Contrast Agents:

In most cases before applying MRI and CT scans intravenous contrast agents are administered. Contrast agents are chemical materials that improve visualization of tissues and body organs. For CT, all contrast agents are iodine-based reagents that absorb and diffract X-rays. There are 13 different CT contrast agents that are FDA-approved. There have been no novel CT contrast agents approved since 1997 [5]. Iodine contrast agents have mild and self-limiting adverse effects in healthy individuals but individuals with impaired renal function can have severe and serious adverse effects including anaphylaxis and nephropathy. Moreover iodine-based contrast agents have short half-lives and rapid clearance, and therefore may require multiple injections [6].

For MRI, most common contrast agents are gadolinium-based (11 types are FDA-approved). Gadolinium ions are paramagnetic and shorten the relaxation time of the excited protons in body tissues and enhance changes in signals between adjacent tissues, which may depend on tissue type or blood flow. Like CT contrast agents, MRI contrast agents are generally safe for all patients except patients with impaired renal function. These contrast agents may develop nephrogenic systemic fibrosis (7).

The existing contrast agents for CT and MRI are effective at enhancing anatomical imaging, but they are not cancer-specific and largely fail to distinguish malignant from

benign lesions. That is why there is an urgent need to develop cancer-targeted contrast agents to diagnose cancer at an early stage. The Molecular Imaging and Contrast Agent Database (MICAD) lists more than 5,000 targeting compounds that have been reported in the literature with around 2,000 for cancer diagnosis. Many cancer-targeted ligands have been tested, such as peptides, antibodies, small molecules, and aptamers. Aptamers have numerous advantages due to ease of synthesis, their nano-size, physical properties, and versatile chemistry.

1.3. Anti-Nucleolin Aptamer AS1411:

AS1411 is a quartet G-rich oligodeoxynucleotide that specifically binds to a phosphoprotein called nucleolin that is overexpressed in almost all cancer cells where it is found on the cell surface and in the cytoplasm. Nucleolin is absent from the cell surface and cytoplasm of almost all normal cells. AS1411 has apoptotic induction activity through binding to nucleolin, which inhibits nucleolin binding to BCL2 mRNA (BCL2 is a family of regulatory proteins that regulate cell apoptosis by either inducing or inhibiting apoptosis). AS1411 is taken up in cancer cells by macropinocytosis, which leads to specific accumulation in cancer cells. The majority of targeted agents in MICAD database are peptides or antibodies, which target specific molecular targets that are expressed in small subset of cancers, whereas AS1411 has a near-universal cancer targeting mechanism because nucleolin is expressed in most cancer types. AS1411 is the first aptamer to be tested in human trials, and it passed phase I and II clinical trials. More than 100 patients were treated with no serious adverse events reported. Moreover, there is some evidence of clinical benefit. However, the response was low due to poor pharmacokinetics (rapid

clearance from the body and serum concentration is not enough to kill most cancer cells) and low potency of AS1411.

1.4. Conjugation of AS1411 with Gold Nanoparticles (GNPs):

Gold nanoparticles (GNPs) are extensively employed as therapeutic and diagnostic platforms in biotechnology-based applications. GNPs have unique dimensions, tunable functionalities on the surface and display controllable drug release. While traditionally, GNPs have been functionalized with therapeutic agents, disease targeting agents or diagnostic/ contrast agents, recent efforts have focused on combining disease targeting, diagnostic technologies and therapeutics into a single theranostic agent.

In this thesis, we propose a theranostic construct using GNPs conjugated with AS1411 (cancer targeting therapeutic aptamer) and gadolinium chelate (Dotarem thiol derivative; Gd (III)-DO3A) as MRI contrast agents [10] (see Figure 2). Conjugation of AS1411 with GNPs has many advantages over using AS1411 alone. AS1411-GNPs have a dramatic increase in uptake by cancer cells (along with up to 50-fold increase in potency against cancer cells) while maintaining cancer selectivity (no effect on normal cells) and display antitumor activity in mice with no evidence of toxicity [9]. Additionally, AS1411 can be easily co-localized to GNPs using a thiol group.

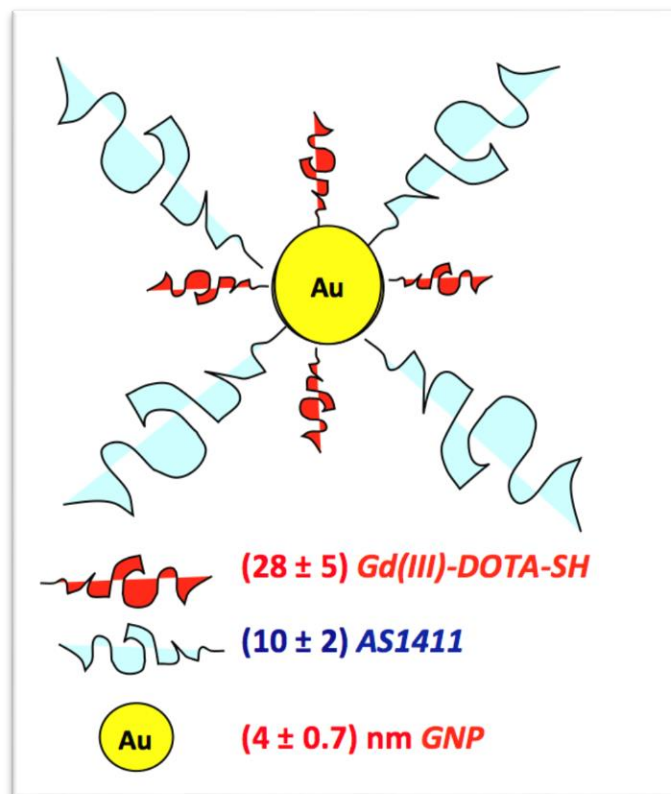


Figure 2: GNP functionalized with Gd (III) DO3A-SH and AS1411.

Gd (III) ions cannot be administered directly in their ionic form because they are very toxic. Gd (III) ions interfere with calcium channel and protein binding sites, and also accumulate in liver, bones, spleen, and kidney. That is why Gd(III) ions are formulated with chelating agents to prevent tissue interaction and minimize their toxic effect [11] (see Figure 3). Here we use DO3A (1,4,7,10-tetraazacyclododecane-N,N',N'',N'''-tetraacetic acid) as chelating agent with a thiol group that allows conjugation of Dotarem to GNPs.

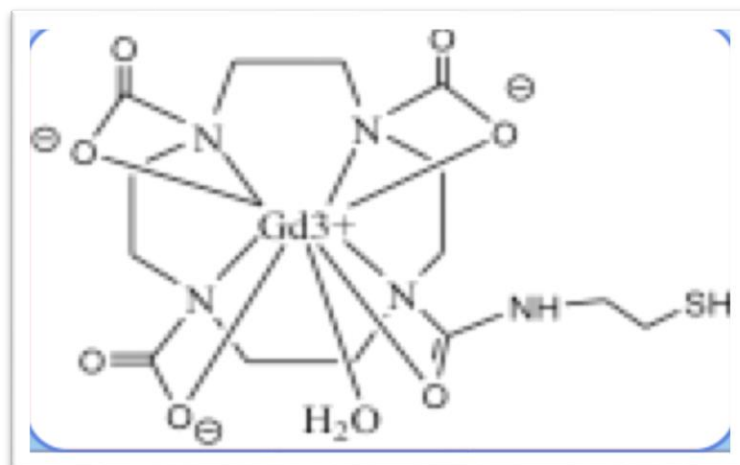


Figure 3: Gd ion is chelating to DO3A with thiol group.

The first goal of this study is to investigate the ability of the proposed contrast agent to enhance the contrast of MRI images using MDA-MB-231 triple negative breast cells line and MCF-10 human mammary epithelial cells line. The second goal is to evaluate the biodistribution and the potential toxicity of the proposed contrast agent in vivo.

and TTTTTT (CTR).

MDA-MB-231 breast cancer cells and MCF-10A healthy mammary gland cells were purchased from ATCC (Manassas, VA). MEMM media with Bullet Kit Media were purchased from Lonza Group (Basel, Switzerland). DMEM, Fetal Bovine Serum (FBS), 10X Trypsin, Penicillin/Streptomycin (Pen/Strep) & Gentamicin were all purchased from Thermo Fisher Scientific (Waltham, MA). Phosphate-buffered saline (PBS) 1X without calcium or magnesium was purchased from Gibco. Accutase solution was purchased from Sigma-Aldrich. (3-(4,5-dimethylthiazol-2-yl)-2,5-diphenyl tetrazolium bromide), MTT reagent was purchased from Sigma (Cream Ridge, NJ). Sodium dodecyl sulfate (SDS) was purchased from Thermo Fisher Scientific. Tissue culture flasks, dishes and plates were purchased from Thermo Fisher Scientific. Amicon Ultra 15.0 ml centrifugal filters with Ultracel-30 (30000 MWCO) were purchased from Merck Millipore (Billerica, MA) to remove excess oligonucleotide and *Gd(III)-DO3A-SH*. The 0.6 ml Eppendorf microcentrifuge tubes were purchased from Sigma Aldrich (St. Louis, MO) to mount samples at 9.4 T (Agilent) MRI scanner.

UV absorption spectra were measured with a UV Visible Spectrometer (Varian Cary 50 BIO UV, Agilent Technologies, Santa Clara, CA). Dynamic Light Scattering measurements (DLS) were acquired on a Zetasizer (Zetasizer Nano ZS90, Malvern Instruments Ltd., Westborough, MA). The Zeta potential measurements were acquired using a NanoBrook Zeta PALS Zeta Potential Analyzer (Brookhaven Instruments, Holtsville, NY). Tunneling electron microscopy (TEM) studies was performed on the FEI Tecnai F20 TEM to determine GNP morphology and distribution. Fluorescence studies were performed on the enhanced darkfield CytoViva fluorescence microscope (CytoViva,

Inc., Auburn, AL).

2.2. Chemical synthesis of 4 nm GNPs:

Gold nanoparticles were synthesized according to the procedure described by Murphy and coworkers [12]. A 2.5 mL of 0.01M citric acid, trisodium salt was added to 95.0 mL of nanopure water under intense stirring. Then, 2.5 mL of 0.01M HAuCl₄ solution was added followed immediately by 3.0 mL of 4°C 0.1M sodium borohydride. The solution was stirred for 2 hours. GNPs size was determined by UV/vis and dynamic light scattering.

2.3. Chemical Synthesis of Gadolinium (*III*) DO3A-SH:

The tetraazamacrocyclic 10-(2-sulfanylethyl)-1,4,7,10-tetraaza cyclododecane-1,4,7-triacetic acid (DO3ASH) was chelated with GdCl₃ by mixing an aqueous solution of DO3A-SH (15.8 μmol, 100 μl) with an aqueous solution of GdCl₃ (347 mM, 50 μL) at room temperature [13-15]. The reaction mixture pH was then adjusted to 6.0 with 1.0 M sodium bicarbonate and the mixture incubated overnight at 60°C. During the reaction, the pH was monitored three times and bicarbonate solution added as necessary to keep the pH in the range of 6-7. Afterwards, the reaction mixture pH was adjusted to 9-10 using sodium bicarbonate and then centrifuged at 3000 g for 15 minutes. The sample was then vacuum filtered and the precipitate air-dried.

2.4. Preparation of AS1411/CRO/CTR for conjugation to GNP:

Oligonucleotides having a regular DNA backbone (phosphodiester), a 5'-Thiol C6 S-S modification (Thio-MC6-D), and high pressure liquid chromatography (HPLC) purified were supplied by Integrated DNA Technologies (IDT). Oligonucleotide solutions were prepared as previously reported [16]. Briefly, 500 μl of 500 μM oligonucleotide

solution was prepared by suspending AS1411/CRO/CTR in nanopure water. Prior to use, the disulfide protecting group on the oligonucleotide solution was cleaved with dithiothreitol (DTT). A 250 μ l solution of 1M DTT was added to 60 μ l of 500 μ M oligonucleotide solution and heated at 90°C for 1 hour (0.1 M DTT, 0.18 M phosphate buffer (PB), pH 8.0). The cleaved oligonucleotides were purified using a NAP-5 column eluted with PB. Thereafter, the eluted solution of freshly cleaved oligonucleotides was added to gold nanoparticle dispersions.

2.5. Chemical synthesis of GNP–Gd(III)-DO3A-SH- Oligonucleotide:

Gold nanoparticles (GNP) were functionalized with the MRI contrast agent Gd(III)-DO3A-SH and/or thiol-deprotected oligonucleotide (AS1411/CRO/CTR). The freshly cleaved oligonucleotide solution was added to the GNP dispersion (~170 nM) [12] to bring the mixture to 1.2 μ M oligonucleotide concentration [16] while simultaneously adding Gd(III)-DO3A-SH to achieve 1.3 mM contrast agent concentration. The GNP-Gd(III)-DO3A-SH-Oligonucleotide solution was incubated at room temperature for 20 minutes and then sonicated for 10 minutes. The solution was incubated overnight at 37°C. The concentration of NaCl was gradually increased to 137 mM using 10X PBS over 3 days. During each salt addition, the GNP-Gd(III)-DO3A-SH-Oligonucleotide solution was sonicated for 60s followed by incubation at 37°C. As mentioned, the excess oligonucleotide and Gd(III)-DO3A-SH were removed via centrifugal filtration at 3000g for 30 min. The concentrated solution was re-suspended to 15.0 ml with 1.0 X PBS and filtered two more times before use.

2.6. Oligonucleotides Quantification:

45.0 μL of the centrifuged pellets of GNP-*Gd(III)DO3A-SH*-Oligonucleotide were redispersed to 2.0 ml samples at 45X dilution in GNP stripping solution (5 μL of 1.0 M DTT, 0.1M phosphate buffer (pH 8)) and incubated overnight at 37 °C to cleave the gold oligonucleotide-thiol bond. Within 24 hours, after the gold nanoparticles precipitate, the supernatant was collected and the released oligonucleotides were quantified using UV absorption spectra.

2.7. Transmission Electron Microscopy:

Transmission electron microscopy (TEM) images were obtained using a FEI Tecnai F20 TEM. A field emission gun (FEG) was used for the electron source and the studies were performed with an accelerating voltage of 360 keV. The samples were prepared by suspending 20.0 μL of 0.5-0.6 μM concentration of GNP samples onto a C-flat holey carbon film mesh on copper grids and air dried overnight. The size histogram analysis of the TEM images was performed with ImageJ software.

2.8. Fluorescence:

The samples (the synthesized GNPS) were tagged with the fluorescent dye OliGreen™ using the protocol provided by the manufacturer. Excess dye was removed through centrifugation at 3000 rpm for 30 min. A Modulus Fluorimeter (Promega, Madison, WI) was used to measure the fluorescence of the samples (Blue module: Ex 460 nm, Em: 518-570 nm). The samples were also imaged with an enhanced darkfield (Cytoviva) fluorescence microscope. The samples were prepared by drop casting 10.0 μL of sample onto a glass microscope slide (Fisherbrand Superfrost Plus) and then placing a

coverslip ovetop (VWR micro cover glass). Lacquer (Nail Polish) was then used to create a waterproof seal around the edges. The samples were imaged at 60x magnification.

2.9. Gadolinium quantification with Energy Dispersive X-Ray Analysis:

Energy Dispersive X-ray Analysis (EDAX) was performed on a Zeiss SUPRA 35 FE-SEM (Zeiss Peabody, MA) at 20 KeV incident beam at 8.1 mm working distance. The atomic ratios of Gd:Au were measured for GNP –*Gd(III)-DO3A-SH*- oligonucleotide to quantify Gd content per GNP.

2.10. Cell Culture development:

MDA-MB-231 and MCF-10A cells were maintain DMEM and MEBM, respectively. Cells were cultured in a 5% CO₂ incubator at 37°C and media were replaced with fresh media every two to three days. Cells were subcultured every four to five days using PBS for MDA-MB-231 and accutase for MCF-10A.

2.11. MRI Agarose Phantoms:

Samples for MRI imaging were prepared by mixing different concentrations (1200, 300 and 75 nM) of gold nanoparticles functionalized with Gd(III)- DO3A-SH and oligonucleotide (AS1411/CRO/CTR) with agarose solution (0.7%, 55°C) in 1:1 ratio in 0.5 mL Eppendorf microcentrifuge tubes. The uniform dispersions were allowed to stand at room temperature for 30 minutes to solidify. Samples were mounted on a mesh grid and MRI images were acquired on the 9.4 T instrument (Agilent) for T1 W and T1 MRI measurements. Concentrations of gold nanoparticles (1200 nM, 300 nM and 75 nM)

functionalized with Gd(III)- DO3A-SH and oligonucleotide (AS1411/CRO/CTR) were diluted in agarose solution (0.7%) and mounted on the 9.4 T instrument holder for their T1 W and T1 MRI measurements.

2.12. MR imaging:

All MR imaging data were acquired using Agilent 9.4 T horizontal bore MRI system equipped with Agilent 205/120 HD gradient coil (Agilent Technologies, Santa Clara, CA, USA). A RAPID 72-mm volume coil was used for signal transmission and detection (RAPID MR International, Columbus, OH, USA). After a quick 3-plane gradient echo-based scout scan to verify sample positioning, T1-Weighted images were obtained using a standard spin echo multi-slice (SEMS) imaging sequence with the following parameters: TR/TE = 500/10 msec; matrix size = 128 x 128; field of view (FOV) = 40 x 40 mm²; 13 slices with a slice thickness of 1.0 mm. When acquiring data for T1 calculation purposes, a fast spin echo multi-slice (fSEMS) sequence was used with the following parameters: TR (array) = 6000, 4700, 3600, 2800, 2200, 1700, 1300, 1000, 800 msec; effective TE = 20 msec; matrix size = 128 x 128; field of view (FOV) = 40 x 40 mm²; 9 slices with a slice thickness of 2.0 mm and 2 averages. All data from 9.4T MRI system were converted to DICOM format using VNMRJ 4.0 interface before transferring to other software for further data processing. Samples were also scanned using a 3 T Siemens MAGNETOM Skyra (Siemens Medical Solutions, Malvern, PA, USA) with a 20 channel head coil. A turbo spin echo (TSE) sequence was used under 3 T for T1 quantification: TR (array) = 5000, 2000, 1000, 750, 500 msec; TE = 10 msec; matrix size = 256 x 256; field of view (FOV) = 18 x 18 cm²; 17 slices with a slice thickness of 1.4 mm.

2.13. Determination of GNP –*Gd(III)-DO3A-SH*- Oligonucleotide cellular uptake using live MDA-MB-231 and MCF-10A:

MDA-MB-231 and MCF-10A were treated with different concentrations of gold nanoparticles (1200 nM, 300 nM, and 75 nM) functionalized with *Gd(III)-DO3A-SH* and AS1411/CRO/CTR made in complete DMEM and MEBM, respectively, and incubated for 24, 48, 72 & 96 hour time points at 37°C to allow cell uptake and localization. After the prescribed incubation time, the media was discarded and cells were washed 3 times with 1X PBS to remove any excess and unbound gold nanoparticles that were not internalized within the cells. Cells were detached from the monolayer using TryPLE and accutase solutions for 5 minutes at 37°C, transferred to a 15 mL conical tube, and centrifuged at 700 rpm to pellet the cells and separate any remaining unbound gold nanoparticles. Excess gold nanoparticles, TryPLE, and accutase solutions were removed and cell pellets were suspended in 100 µl of 1X PBS, and transferred to 0.5 mL tubes with the addition of 100.0 µl of 1.4% agarose to give a final concentration of 0.7% agarose for a clear homogenous solution. Cells were then mounted on the 9.4 T instrument mesh grid holder for T1-Weighted and T1 MRI measurements.

2.14 T1-Weighted image analysis algorithm:

The T1-Weighted image calculation algorithm starts with single-click selection of the two Eppendorf microcentrifuge tubes (0.5 ml) to be analyzed (see Fig. S5 (a)). Then a background removal and a 3D region-growing algorithm is applied to extract the volume of interest (VOI) that contains each microcentrifuge tube (0.5 ml) in the middle of the VOI (see Fig.S5 (b-f)). The second step is to perform a two-step 3D registration technique to

guarantee a voxel-on-voxel match between sample and control for accurate relaxivity calculations. The registration technique begins with a global alignment using a 3D affine transformation model. In order to perform the global registration, the distance maps inside the reference and target microcentrifuge tubes (0.5 ml) are generated by finding the minimum Euclidean distance for every inner voxel to the object boundary using a fast marching level set. Then a 3D affine transformation with 12 degrees of freedom is applied to align the target microcentrifuge tube (0.5 ml) to the reference one by maximizing the mutual information of the generated distance maps. The second registration step is to perform a non-rigid alignment (a step confirming voxel on voxel match) using a multiresolution elastic registration approach which is based on 3D cubic B-splines with four-stage multiresolution and using limited memory Broyden-Fletcher-Goldfarb-Shanno (L-BFGS-B) optimization [19].

The traditional method to calculate the relaxivity is as follows:

$$\text{Change in Relaxivity } (R) = \frac{(\text{Test})_{avr} - (\text{Control})_{avr}}{(\text{Control})_{avr}} * 100 \quad (1)$$

Since after aligning the MRI data, we have voxel-on-voxel match, then the proposed equation to calculate the relaxivity is as follows:

$$\text{Change in Relaxivity } (R) = \frac{\sum_{i=1}^N (I_i)_{test} - (g_i)_{control}}{\sum_{i=1}^N (g_i)_{control}} \times 100 \quad (2)$$

Where N is the number of voxels in each image, I_i is the MRI signal of the test cells and g_i is the MRI signal of control cells as demonstrated in Figure 4.

Note that each MR scan has one microcentrifuge tube (0.5 ml) filled with water. All our data from any MRI scan is divided by the average signal of water. Finally, after calculating

the relaxivity using Eq. 2, the proposed approach generates the color map that shows the relaxivity of each voxel as shown in Figure 5.

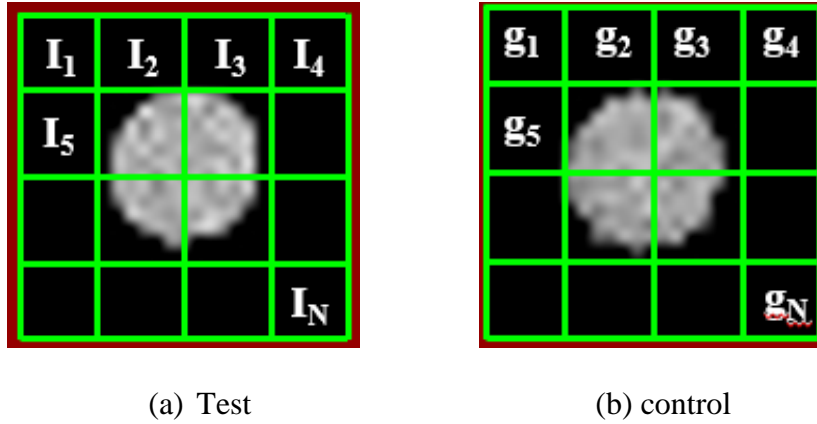


Figure 4: Illustration of the proposed relaxivity calculation.

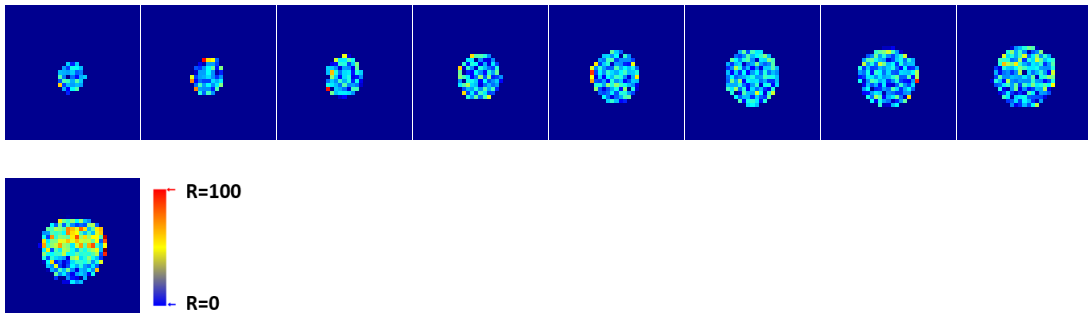


Figure 5: An illustration of color map generated of relaxivity enhancement. Red color means 100% improvement in the relaxivity as demonstrated in the color coded bar.

2.15. In vivo Biodistribution and Toxicity study:

All animal experiments were approved by the Institutional Animal Care and Use Committee (IACUC) at the University of Louisville. Fifty healthy female Sprague Dawley rats (4 weeks old) were purchased from Charles River Laboratories (Wilmington, MA). Rats were fed a standard chow diet and water for the entire duration of the experiment. At

6 week ages, blood samples were collected from the saphenous vein of all animals to be used as a baseline control. On day 2, the animals were randomly divided into 5 groups and injected through tail vein with GNPs coated with *Gd(III)- DO3A-SH* and/or thiol-deprotected oligonucleotides (AS1411, CRO (an analog of AS1411 with all G's replaced with C's), and CTR (a short sequence of thymidylates), MultiHance (Gadobenate Dimeglumine Injection), or saline (MultiHance and saline were used as controls). Rats were euthanized using CO₂ and blood samples were collected through Cardiac Puncture using 23G one inch syringes after two or fourteen days from each group. Blood samples were centrifuged (800g) to collect 200 µl of serum for the general health profile chemistry panel and organs were collected and stored in 10% formalin for ICP-MS analysis.

(a) Inductively Coupled Plasma Mass Spectrometry (ICP-MS):

The sample preparation for ICP-MS/MS analysis consisted of a microwave acid digestion of the collected tissue. The samples (about 80-200mg) were placed into 10 ml Pyrex digestion vials, 2 ml of concentrated trace metal grade nitric acid was added, and samples were kept at room temperature for 2 hours as pre-digestion step. Then 0.5 ml of 1:1 hydrochloric acid and 20 ml of internal standard solution containing Indium was added and the closed vials were microwaved in a CEM Discovery digestion system. The temperature program consisted on a 10 minute ramp to 110 °C with one minute holding followed by a 10 minute ramp to 195 °C with a 15 minutes holding time. The maximum pressure was set at 295 PSI and the maximum power of 300 Watts.

Once the digestion was completed the samples were brought to a final volume of 20 ml with doubly deionized water for a final concentration of 10 ppb of the internal

standard before the analysis.

The total element analysis was carried out using an Agilent ICP-MS/MS system. It consisted on a SPS 4 Autosampler, a micromist quartz nebulizer, a Double pass Scott spray chamber cooled to 2°C, a 2.5 mm ID standard torch, nickel sampler and skimmer cones. The quantification was performed by the external calibration method with gold and gadolinium standards in the 0.5 to 200 ppb range with Indium used as internal standard at a concentration of 10 ppb. For the calibration, R values of 0.9990 or larger and blank equivalent concentration lower than 50 ppt were obtained for both elements.

The analysis was performed for the following isotopes: ^{197}Au , ^{157}Gd and ^{155}In . The integration time per isotope was set at 0.1 s, and the probe rinsing program consisted on a 10% nitric acid followed by 5% HCl solutions.

(b) General Health Profile Chemistry Analysis:

Blood chemistry analysis (General Health Profile) was performed on 50 Sprague Dawley (CrI:SD) rats. Blood was taken before treatment exposure and after (day 2 and day 14) after euthanasia. The GHP was performed at U of L through Research Resource Center (RRC) and detects the following: alkaline phosphate (ALP), alanine transaminase (ALT), creatinine (CREA), total bilirubin (TBIL), and blood urea nitrogen (BUN).

For the baseline measurements (before treatment), the blood volume taken from the rats (6 weeks old) was 100ul for each rat through the saphenous vein. After blood collection, the blood was centrifuged to collect 40 μl of serum which was needed for the GHP analysis (minimum detection limit). After euthanasia (day 2 or 14), blood collection was performed through the heart's atrium yielding around 1 ml. This allowed for a higher

volume of serum (200 μ l) to be collected and analyzed through the GHP.

2.16 Statistical Analysis:

For blood chemistry results, we performed two statistical tests to analyze the data that were collected. The first test is based on using unpaired t-test by assuming all the involved biomarkers in this experiment are independent. The second statistical test is based on using ANOVA test in order to make group analysis in case the collected biomarkers are dependent/correlated. For both tests we calculated the p-value to determine if there is the significant change in the measured biomarkers that they may related to the toxic effect of the particles. Differences in data were considered significant if p values...less than 0.05.

CHAPTER 3: RESULTS AND DISCUSSION

3.1 Characterization of solutions of GNP and GNP *Gd(III)DO3A-SH* Oligonucleotide:

Dynamic light scattering (DLS) was measured to determine the size distribution profile of the particles and hydrodynamic size in solutions of GNP and GNP *Gd(III)DO3A-SH* oligonucleotide. Transmission electron microscopy (TEM) was used to determine the size of gold nanoparticles GNP and GNP *Gd(III)DO3A-SH* oligonucleotide. Zeta Potential were measured to determine particles stability for solutions of citrate capped GNP and GNP *Gd(III)DO3A-SH* oligonucleotide.

Table 1: DLS, TEM, Zeta Potential characterization of citrate capped GNP and GNP *Gd(III) DO3A-SH* Oligonucleotide.

Sample	Hydrodynamic size (nm)	TEM (nm)	Zeta Potential (mV)
GNP <i>Gd(III) DO3A-SH</i> AS1411	13.5 ± 2.1	3.4 ± 0.6	-20.9 ± 1.1
GNP <i>Gd(III) DO3A-SH</i> CRO	19.3 ± 2.5	3.3 ± 0.6	-57.6 ± 1.0
GNP <i>Gd(III) DO3A-SH</i> CTR	9.83 ± 1.45	5.45 ± 1.42	-42.67 ± 4.15
GNP Citrate	4.88 ± 0.51	4.0 ± 0.7	-16.25 ± 2.30

Table 1 shows that the compact monomeric quadruplex formation of AS1411 leads

to the relatively smaller hydrodynamic diameter of GNP-*Gd(III)*-*DO3A-SH*-AS1411 (13.5 ± 2.1) in comparison to GNP-*Gd(III)*-*DO3A-SH*-CRO (19.3 ± 2.5). A zeta (ζ) potential of $-(58 - 20)$ mV was observed for GNP *Gd(III)**DO3A-SH* Oligonucleotide solutions, which displayed high stability and resistance to aggregation in PBS dispersions. On the other hand, the citrate capped gold nanoparticles (GNP) aggregated in PBS dispersions and therefore zeta (ζ) potential and hydrodynamic size characterizations were performed in nanopure water.

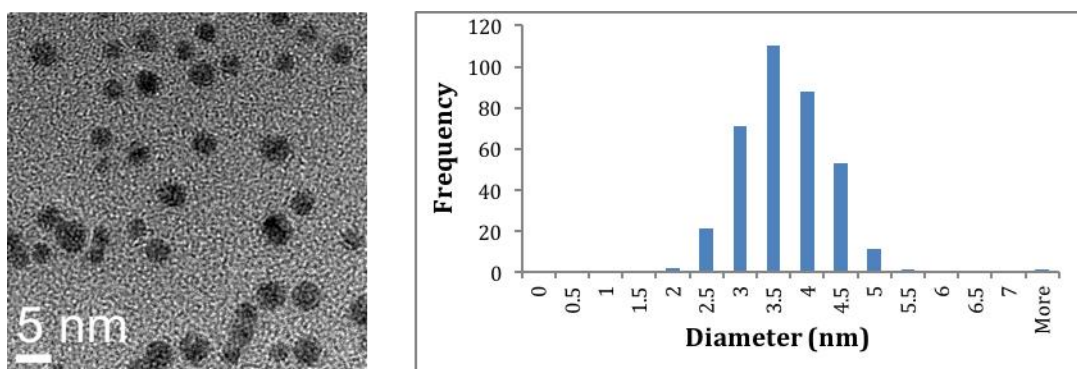


Figure 6: TEM image and particle size histogram for GNP-*Gd-DO3A-SH*-AS1411 (n=500)

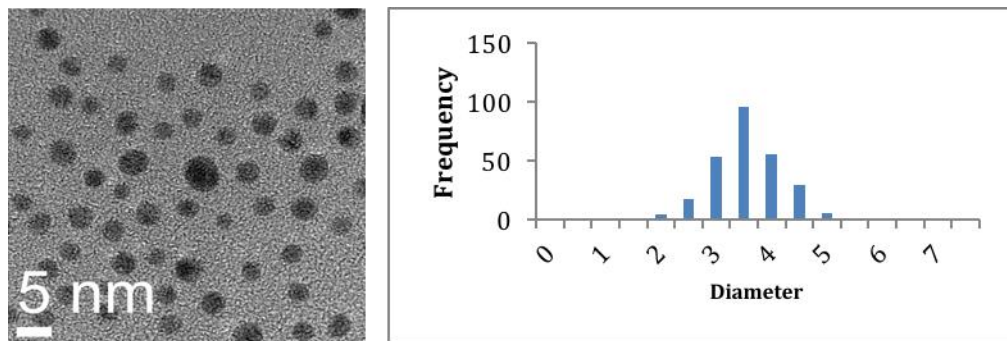


Figure 7: TEM image and particle size histogram for GNP-*Gd-DO3A-SH*-CRO (n=500)

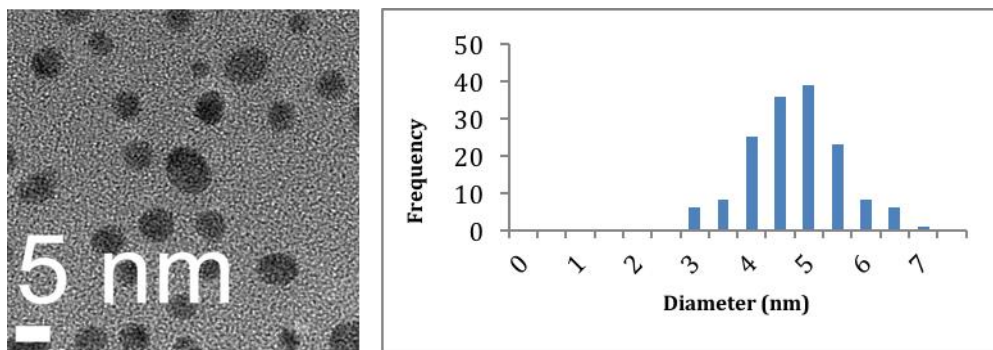


Figure 8: TEM image and particle size histogram for GNP-*Gd-DO3A-SH-CTR* (n=500)

Figures 6-8 show that TEM images of GNP-*Gd(III)DO3A-SH-Oligonucleotide* (AS1411/CRO/CTR) reveal average gold core diameters of (3-6) nm. Although the particles are coated with aptamer and contrast agent, only the gold core of the particles is electron dense enough to have contrast in this imaging technique using formvar coated sample grids. TEM characterizations were performed in nanopure water. Citrate-capped GNP and GNP-*Gd(III)DO3A-SH Oligonucleotide* solutions were stable for more than 6 months in solution at 4°C and 37°C, respectively based on UV-vis measurement.

3.2. Oligonucleotides Determination and quantification:

(a) OliGreen Fluorescence and Darkfield microscopy:

As demonstrated in table 2, three samples solution were stained with OliGreen dye. GNP *Gd(III) DO3A-SH*, 1 X PBS Buffer, and GNP *Gd(III) DO3A-SH AS1411* to determine the presence of oligo in the samples. The test solution (GNP *Gd(III) DO3A-SH AS1411*) has a higher reading (3988.6 FLU) in comparison to GNP *Gd(III) DO3A-SH*

Table 2: OliGreen staining fluorescence values (FL) obtained for GNP Samples using Blue Module (*Excitation* 460 nm; *Emission* 515-570 nm).

Samples	Fluorescence (FLU)
GNP <i>Gd(III)</i> <i>DO3A-SH</i> AS1411	3988.6
GNP <i>Gd(III)</i> <i>DO3A-SH</i>	37.5
1 X PBS Buffer	74.6

OliGreen tagged GNP-*Gd(III)* *DO3A-SH*-AS1411, GNP-*Gd(III)*-*DO3A-SH*, and non-OliGreen tagged GNP-AS1411 were imaged using dark field fluorescence microscopy (see figure 9). The left side of the figure demonstrates gold nanoparticles images. While the right sides demonstrates OliGreen-tagged particles.

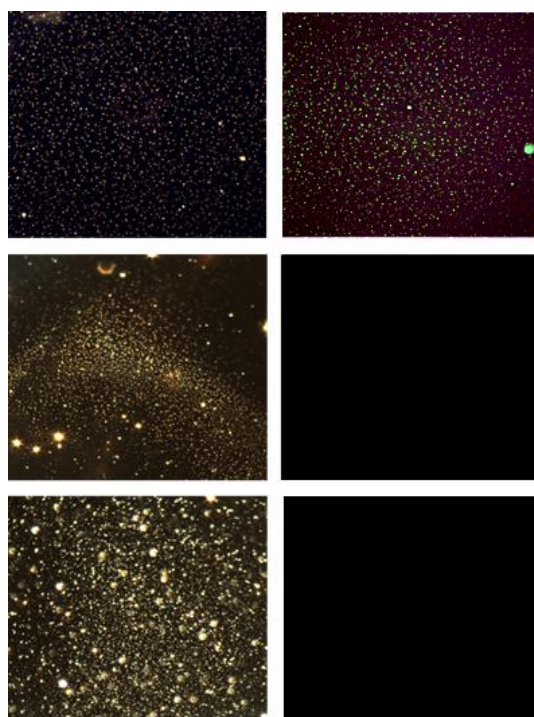


Figure 9: Darkfield (Left) and Fluorescence (Right) characterization of OliGreen tagged GNP-*Gd(III)* *DO3A-SH*-AS1411(Top), GNP-*Gd(III)*-*DO3A-SH* (middle) and non-OliGreen tagged GNP-AS1411 (Bottom).

(b) UV-visible Absorption Spectra Method:

The concentration of oligonucleotides ($\lambda_{\max} = 280 \text{ nm}$) and gold nanoparticles ($\lambda_{\max} = 530 \text{ nm}$) were calculated using Beer's Law equation ($A = \epsilon L c$; A is the absorbance, ϵ is the molar extinction coefficient, (extinction coefficient values: 3620000, 323500, 268800, 49200 L(mole.cm) for 4nm gold nanoparticles, AS1411, CRO, CTR respectively), L is the path of length of the cell holder, and c is the concentration)[20][21]. Then the number of oligonucleotides per gold nanoparticle was calculated by dividing the concentration of oligonucleotides by the concentration of gold nanoparticles.

Table 3: Number of oligonucleotides per gold nanoparticles for two aliquots.

Sample	Quantification of Oligonucleotides
GNP <i>Gd(III) DO3A-SH</i> AS1411	10 ± 2
GNP <i>Gd(III) DO3A-SH</i> CRO	9 ± 2

3.2 Gadolinium quantification:

Gadolinium and gold were quantified using Energy Dispersive X-Ray Analysis (EDAX). The sample is bombarded with an electron beam, which leads to electron transfer. The transferring electrons must give up some of their energy by emitting an X-ray. Each atom of every element releases a unique amount of X-ray during electron transferring process.

An EDX spectrum demonstrates peaks corresponding to the energy levels for which the most X-rays had been received. Each of these peaks is unique to an atom, and therefore corresponds to a single element. The higher a peak in a spectrum, the more concentrated the element is in the specimen.

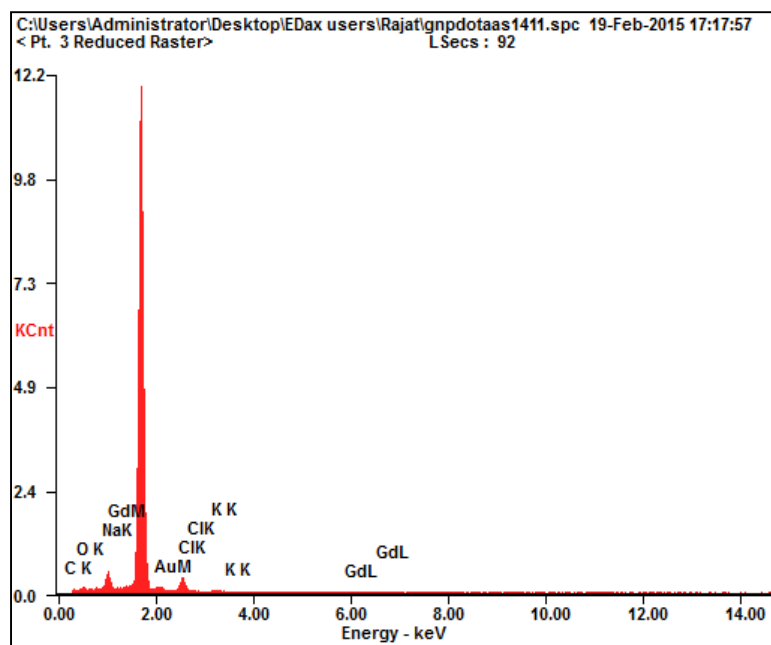


Figure 10: Energy Dispersive X-Ray Spectrum of GNP Gd(III) DO3A-SH AS1411

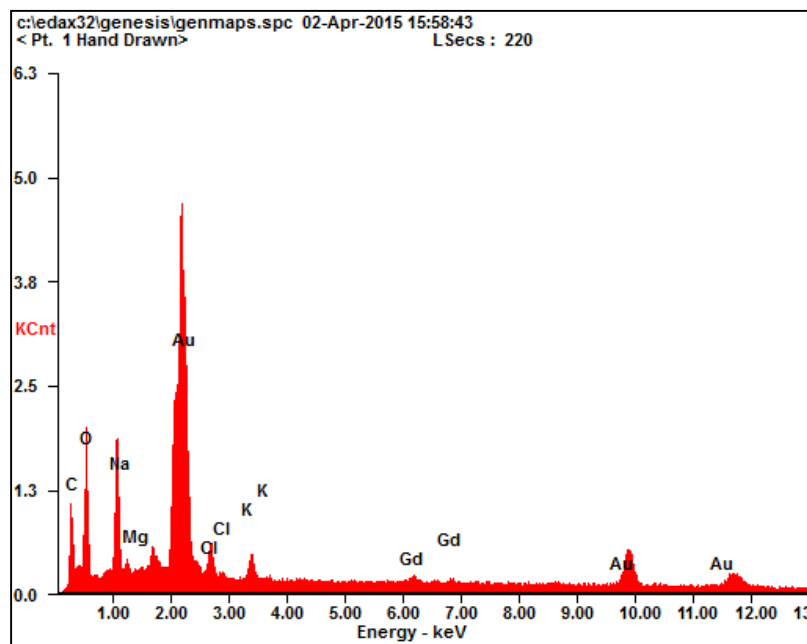


Figure 11: Energy Dispersive X-Ray Spectrum of GNP-Gd(III)DO3A-SH-CRO

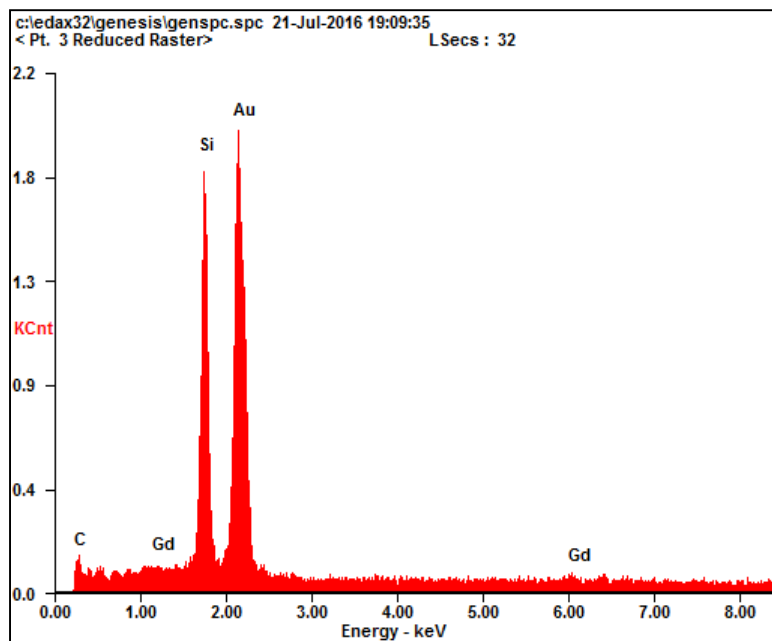


Figure 12: Energy Dispersive X-Ray Spectrum of GNP-*Gd(III)DO3A-SH-CTR*

Figures 10-12 demonstrate the quantification of gadolinium using Energy Dispersive X-ray Assay (EDAX), the spectrum of three samples GNP-*Gd(III)DO3A-SH-AS1411*, GNP-*Gd(III)DO3A-SH-CRO*, and GNP-*Gd(III)DO3A-SH-CTR*. X-ray counts were plotted vs. energy (in keV). Energy peaks coincide with the various elements in each sample.

Table 4: Atomic and Weight percentages of elements analyzed in Energy Dispersive X-Ray Analysis of GNP Gd(III) DO3A-SH AS141.

<i>Element</i>	<i>Wt. %</i>	<i>At %</i>
<i>C K</i>	21.34	38.95
<i>O K</i>	16	21.93
<i>NaK</i>	27.57	26.29
<i>AuM</i>	15.06	1.68
<i>ClK</i>	14.95	9.24
<i>K K</i>	2.88	1.61
<i>GdL</i>	2.21	0.31

Table 5: Atomic and Weight percentages of elements analyzed in Energy Dispersive X-Ray Analysis of GNP-*Gd(III)DO3A-SH-CRO*

<i>Element</i>	<i>Wt. %</i>	<i>At%</i>
<i>CK</i>	27.13	52.39
<i>OK</i>	22.84	33.11
<i>NaK</i>	8.04	8.11
<i>MgK</i>	0.62	0.59
<i>ClK</i>	0.89	0.58
<i>KK</i>	0.67	0.4
<i>GdL</i>	4.02	0.59
<i>AuL</i>	35.78	4.21

Table 6: Atomic and Weight percentages of elements analyzed in Energy Dispersive X-Ray Analysis of GNP-*Gd(III)DO3A-SH-CTR*

<i>Element</i>	<i>Wt. %</i>	<i>At %</i>
<i>C K</i>	7.85	40.77
<i>SiK</i>	15.6	34.64
<i>AuM</i>	71.99	22.79
<i>GdL</i>	4.55	1.8

Tables 4-6 show the atomic and weight percentages of elements in each sample. The atomic and weight percentages of Au and Gd per each gold particles are calculated for GNP-*Gd(III)DO3A-SH-As1411*, GNP-*Gd(III)DO3A-SH-CRO*, GNP-*Gd(III)DO3A-SH-CTR* solutions.

3.3 MRI Phantom:

To evaluate contrast enhancement by GNP-*Gd(III)DO3A-SH-Oligonucleotide*, the longitudinal *T1* relaxation and *T1*-Weighted measurements were made at nanomolar GNP

concentrations (1200, 300, 75 nM) and compared with GNP-SH-Oligonucleotides as a control (figure 13)

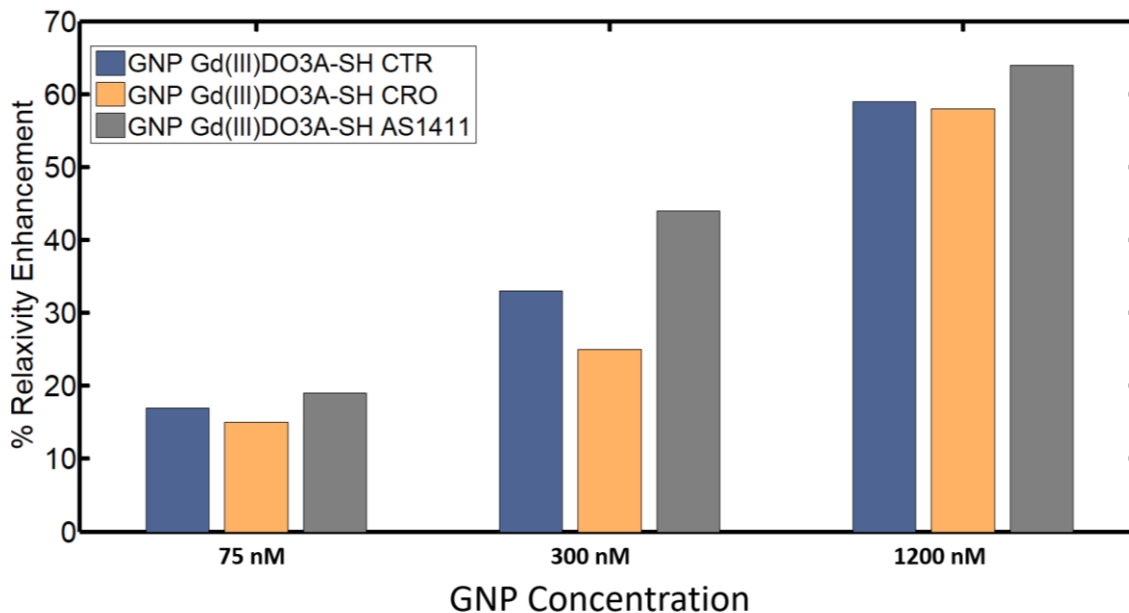


Figure 13: T1-Weighted contrast enhancement comparison for GNP *Gd(III)DO3A-SH* Oligonucleotide.

The % Relaxivity enhancement was calculated as described in the method section. As demonstrated in Figure 10, as we increase the concentration of GNP-*Gd(III)DO3A-SH*-Oligonucleotide there is increase in the percentage of relaxivity enhancement.

3.4 In vitro imaging results:

To evaluate the selective targeting induced contrast enhancement by GNP-*Gd(III)DO3A-SH*-Oligonucleotide, the longitudinal *T1* relaxation and *T1*-Weighted measurements were made at nanomolar GNP concentrations (1200, 300, 75 nM) and compared with corresponding clinically relevant Multihance concentrations (1700, 7000,

27900 nM) in breast cancer cells (MDA-MB-231) and non-malignant breast epithelial cells (MCF-10A). For control experiments with MultiHance, the concentrations (1700, 7000, 27900 nM) were obtained by quantifying the Gd content per GNP using Energy Dispersive X-Ray (EDAX) analysis procedures (17, 18). The atomic ratios of Gd:Au were subsequently measured to quantify Gd content per GNP. MRI scans were applied to the treated cells after incubation for four time intervals (24, 48, 72, and 96).

Table 7: T1-Weighted contrast enhancement comparison for GNP *Gd(III)DO3A-SH* Oligonucleotide in MDA-MB-231 & MCF-10A cell lines using T1-Weighted image analysis algorithm, * *A = AS1411*, *B = CRO*, *C = CTR*, ** M = MultiHance

T1-Weighted Contrast Enhancement (Algorithm)																
Time (Hours)	96				72				48				24			
Cell Lines (type) with GNP Concentration (nM)	* GNP <i>Gd(III)DO3A-SH</i> Oligonucleotide			**M	* GNP <i>Gd(III)DO3A-SH</i> Oligonucleotide			**M	* GNP <i>Gd(III)DO3A-SH</i> Oligonucleotide			**M	* GNP <i>Gd(III)DO3A-SH</i> Oligonucleotide			**M
	A	B	C		A	B	C		A	B	C		A	B	C	
MDA-MB-231(1200 nM)	42.0	20.6	3.6	4.2	49.2	20.9	5.7	6.7	47.0	25.0	4.1	6.9	24.3	19.2	6.8	7.3
MDA-MB-231 (300 nM)	9.5	4.1	3.1	2.8	29.4	11.7	4.3	5.1	20.0	16.0	3.5	5.8	15.2	10.5	3.8	6.1
MDA-MB-231 (75 nM)	8.6	3.2	2.9	0.8	20.9	8.5	3.9	1.5	9.0	8.0	3.4	4.8	2.2	1.1	0.7	5.4
MCF-10A (1200 nM)	11.0	26.3	15.4		14.4	27.4	13.1		9.1	14.5	7.0		8.5	13.6	7.0	
MCF-10A (300 nM)	9.5	21.2	11.9		11.9	23.7	10.3		6.5	11.1	5.1		5.7	6.8	4.9	
MCF-10A (75 nM)	3.0	11.6	7.0		8.9	19.1	5.5		3.0	6.2	4.5		2.7	6.7	4.1	

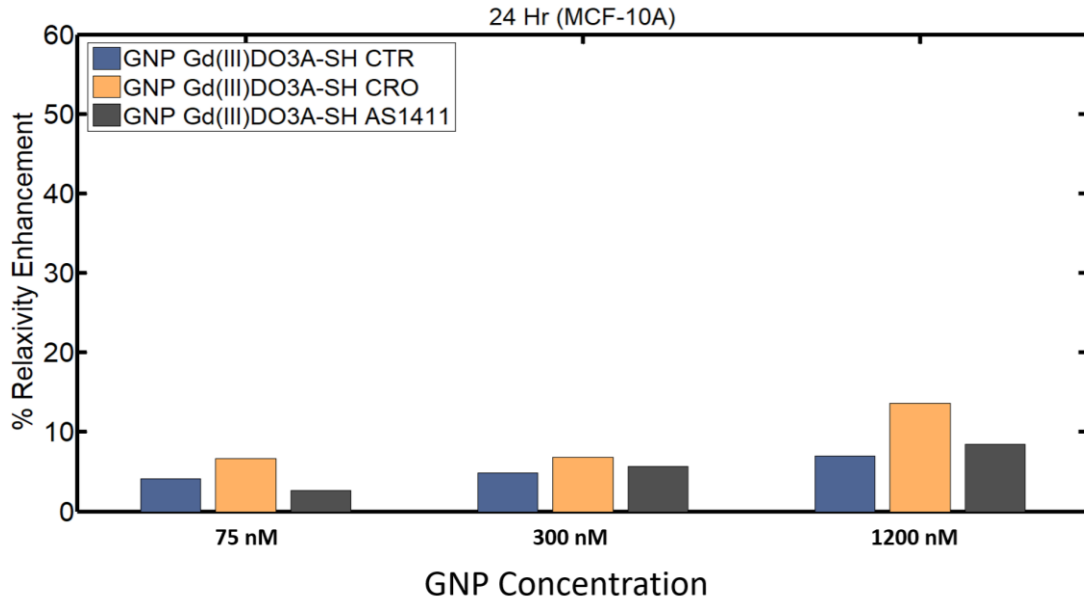


Figure 14: T1-Weighted contrast enhancement comparison for GNP *Gd(III)DO3A-SH* Oligonucleotide in MCF-10A cell line using T1-Weighted image analysis algorithm after

24 hours.

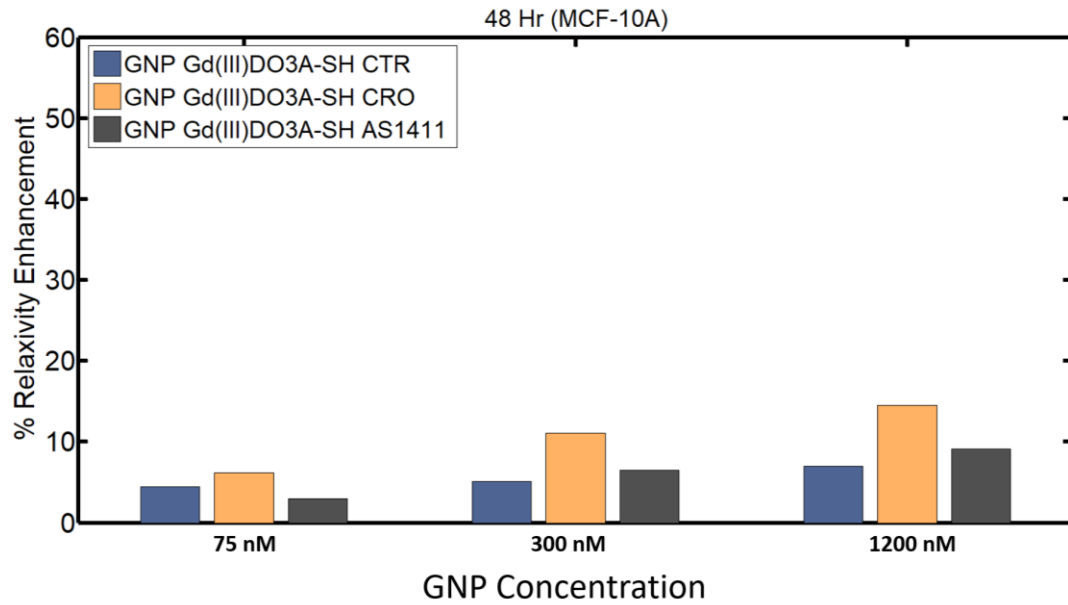


Figure 15: T1-Weighted contrast enhancement comparison for GNP *Gd(III)DO3A-SH* Oligonucleotides in MCF-10A cell line using T1-Weighted image analysis algorithm

after 48 hour.

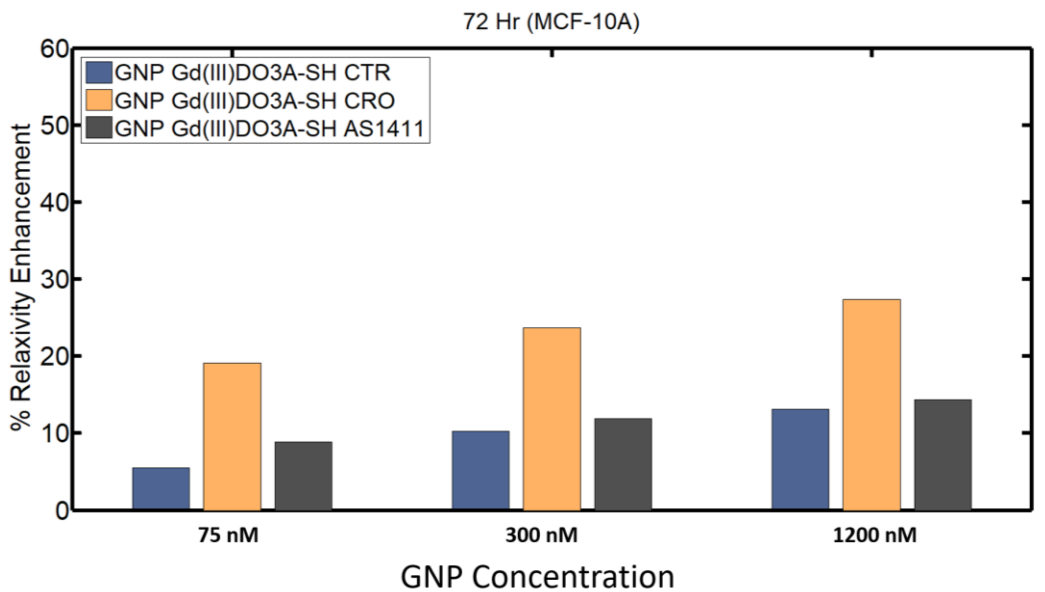


Figure 16: T1-Weighted contrast enhancement comparison for GNP *Gd(III)DO3A-SH* Oligonucleotide in MCF-10A cell line using T1-Weighted image analysis algorithm after 72 hours.

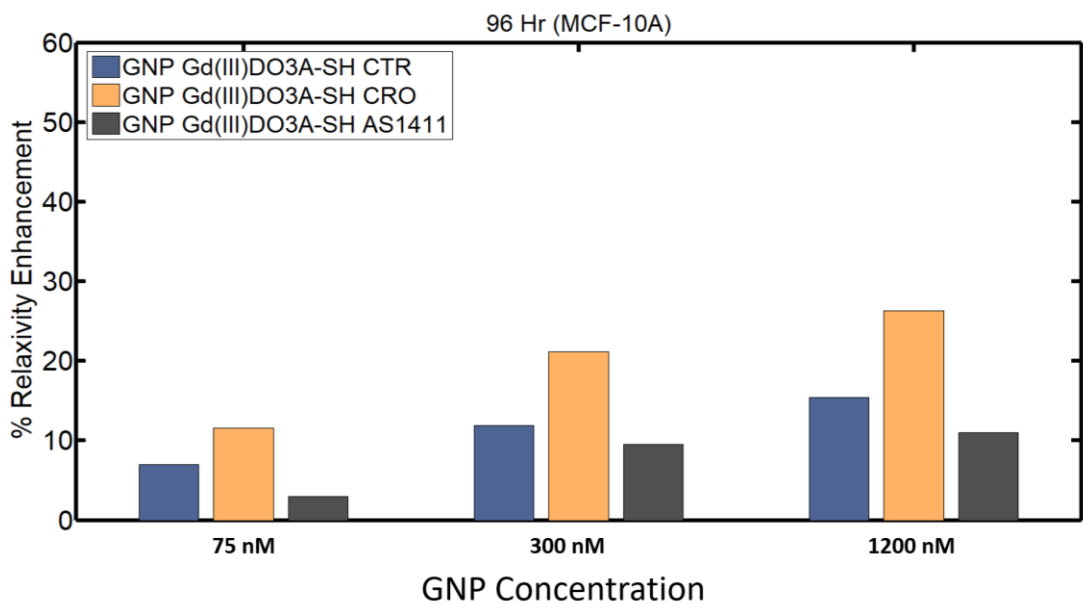


Figure 17: T1-Weighted contrast enhancement comparison for GNP *Gd(III)DO3A-SH* Oligonucleotide in MCF-10A cell line using T1-Weighted image analysis algorithm after 96 hours.

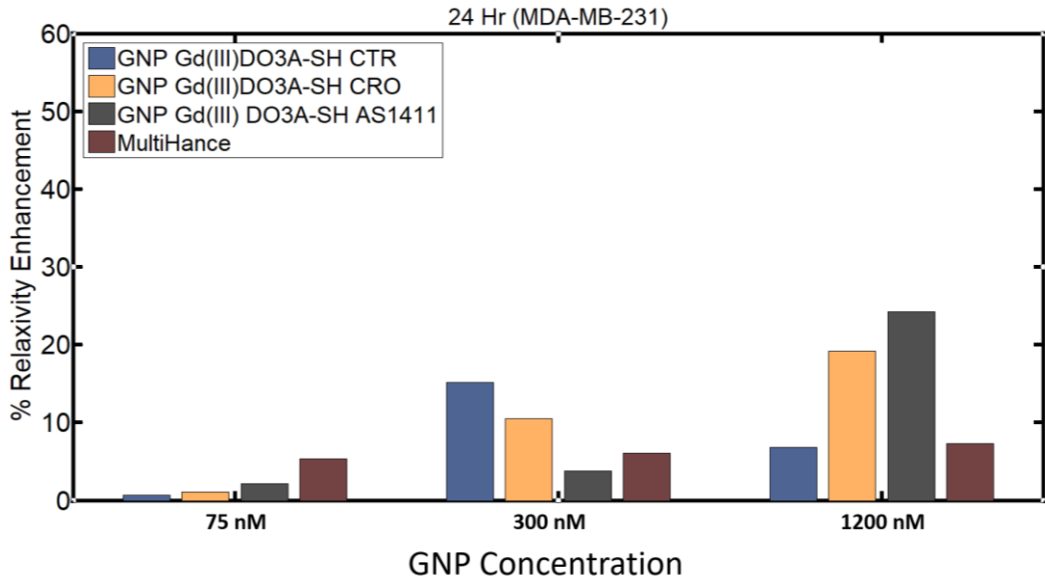


Figure 18: T1-Weighted contrast enhancement comparison for GNP *Gd(III)DO3A-SH* Oligonucleotide in MDA-MB-231 cell line using T1-Weighted image analysis algorithm after 24 hours.

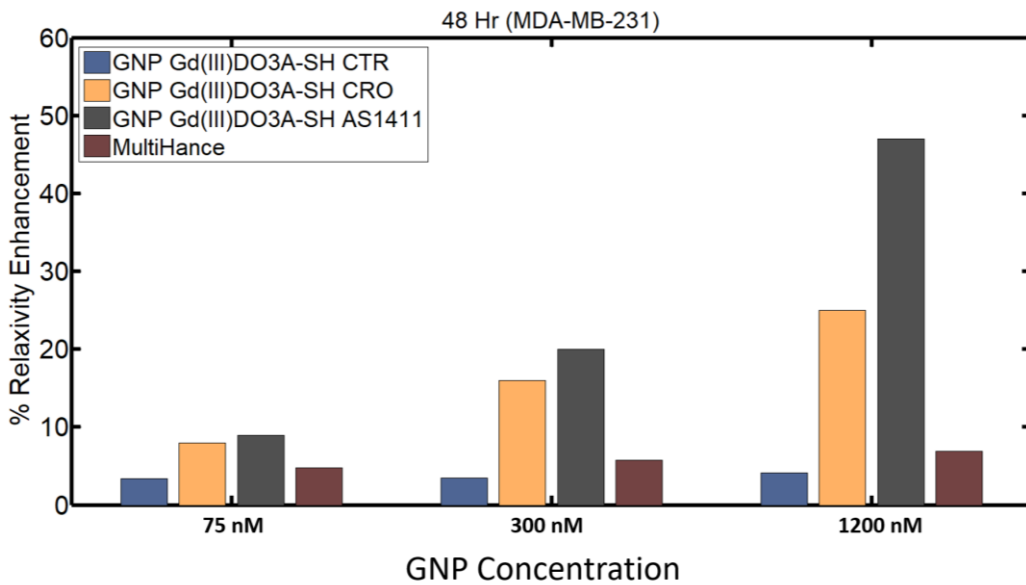


Figure 19: T1-Weighted contrast enhancement comparison for GNP *Gd(III)DO3A-SH* Oligonucleotide in MDA-MB-231 cell line using T1-Weighted image analysis algorithm after 48 hours.

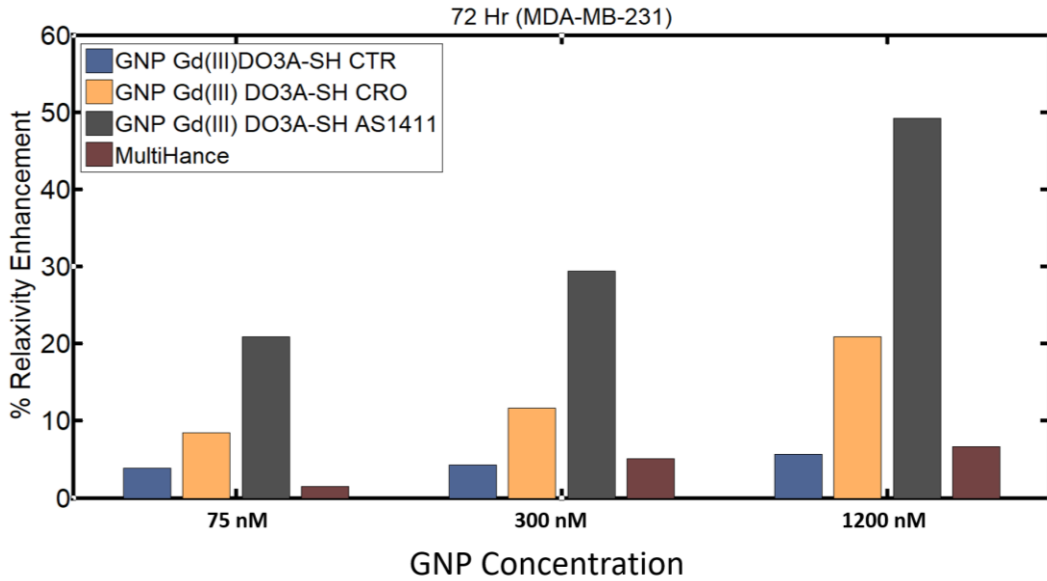


Figure 20: T1-Weighted contrast enhancement comparison for GNP *Gd(III)DO3A-SH* Oligonucleotide in MDA-MB-231 cell line using T1-Weighted image analysis algorithm after 72 hours.

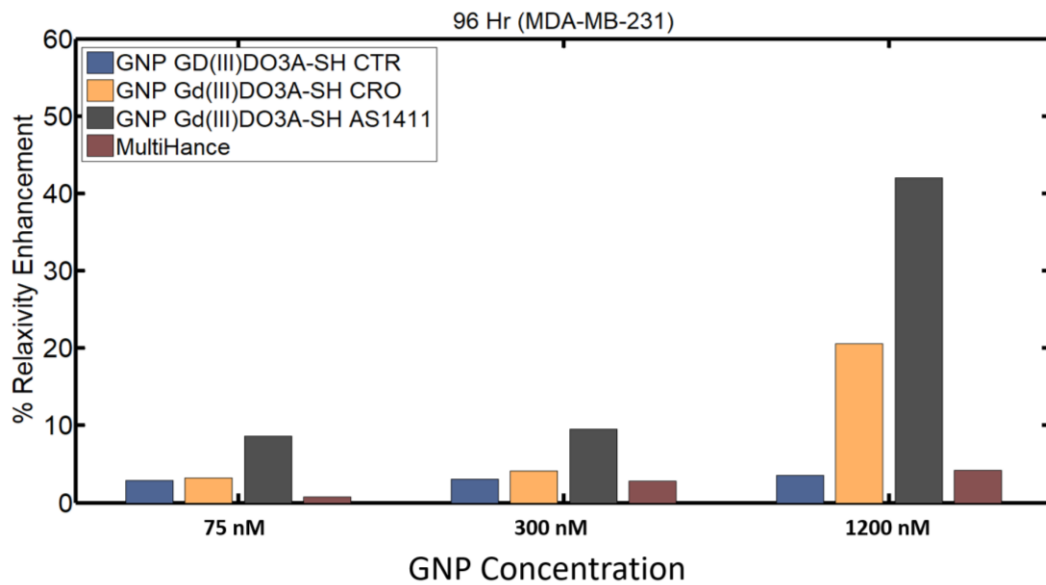


Figure 21: T1-Weighted contrast enhancement comparison for GNP *Gd(III)DO3A-SH* Oligonucleotide in MDA-MB-231 cell line using T1-Weighted image analysis algorithm after 96 hours.

As demonstrated in table 7 and figures 14-21 the enhancement of MRI relaxivity using GNP *Gd(III)DO3A-SH* Oligonucleotide is higher for MDA-MB-231 images than MCF-10A images upon the selective accumulation in cancer cells. MRI images were analyzed using T1-Weighted image analysis algorithm (as described in the methods section), Samples of GNP-*Gd(III)DO3A-SH-AS1411/CRO* display significantly higher relaxivity values compared to GNP-*Gd(III)DO3A-SH-CTR* at 24 hours. While GNP-*Gd(III)DO3A-SH-AS1411* displays the highest enhancement of relaxivity values at 48, 72, 96 hours upon selective targeting (and retention inside) of cancer cells upon binding with nucleolin protein which is highly expressed in the cytoplasm and cell surface (highest enhancement achieves at 72 hours).

3.4 In Vivo Biodistribution Study:

(a) Inductively Coupled Plasma Mass Spectrometry (ICP-MS) Results:

The biodistribution of gold nanoparticles in seven organs (brain, heart, lung, large intestine, kidney, spleen, and liver) had been investigated by ICP-MS. Seven organs were collected after the injection of the five treatment groups by 2 or 14 days.

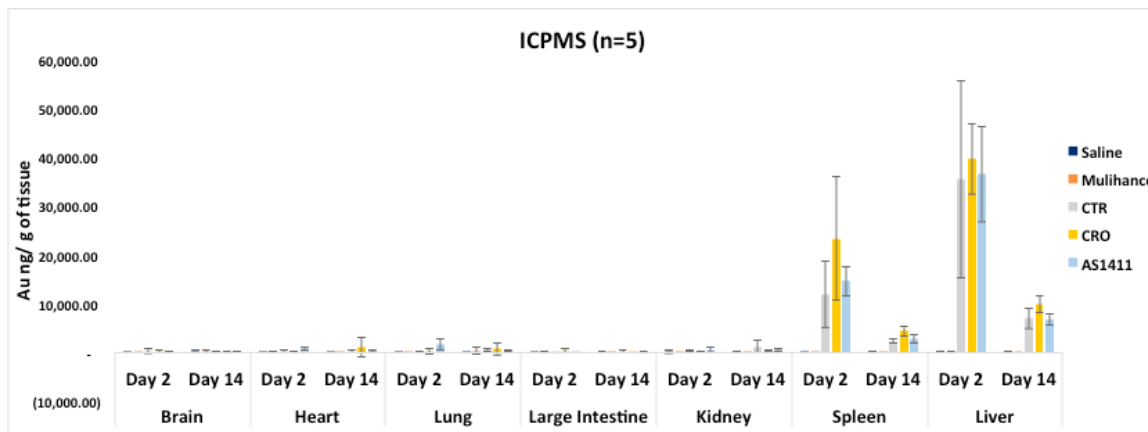


Figure 22: Uptake and biodistribution of gold in different body organs.

- To simplify the figures, CTR stands for GNP *Gd (III) DO3A-SH* CTR, CRO stands for GNP *Gd (III) DO3A-SH* CRO, and AS1411 stands for GNP *Gd (III) DO3A-SH* AS1411.

ICP-MS results show the biodistribution of gold nanoparticles in seven organs (brain, heart, lung, large intestine, kidney, spleen, and liver) of 50 rats after injection with GNP-*Gd(III)DO3A-SH*- oligonucleotides, saline, and MultiHance. Animals were sacrificed after 2 and 14 days of injections. The liver and spleen show the highest concentration of gold nanoparticles with respect to other organs. Moreover, the concentrations of the particles on day 14 are less than the concentrations in day 2 for both organs, suggesting ongoing clearance of nanoparticles from these organs.

(b) Blood Chemistry Analysis:

Blood samples were drawn from the rats after treatment with GNP *Gd (III) DO3A-SH* AS1411, GNP *Gd (III) DO3A-SH* CRO, GNP *Gd (III) DO3A-SH* CTR, MultiHance, and Saline for blood analysis at 2 time points (2 or 14 day). Five blood biomarkers (BUN, ALT, ALKP, CREA, and TBIL) were chosen to evaluate liver and kidney functions.

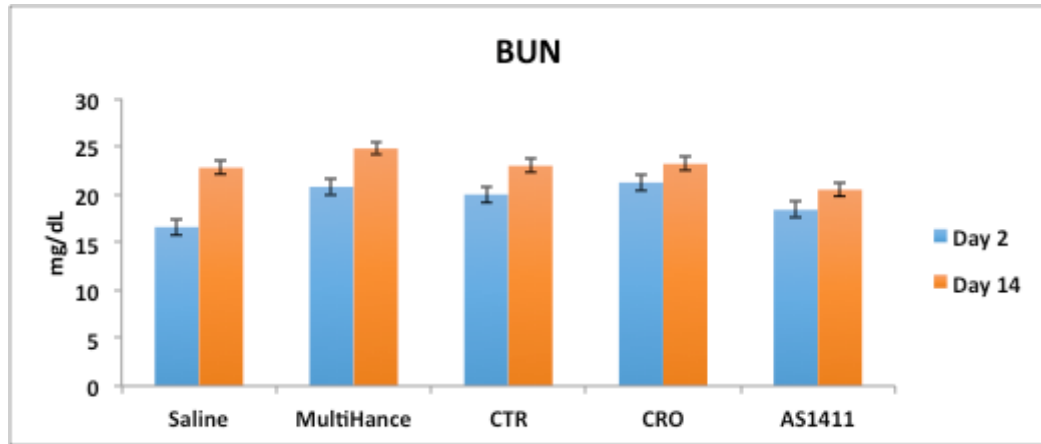


Figure 23: BUN post-treatment blood concentrations of 5 treatment groups.

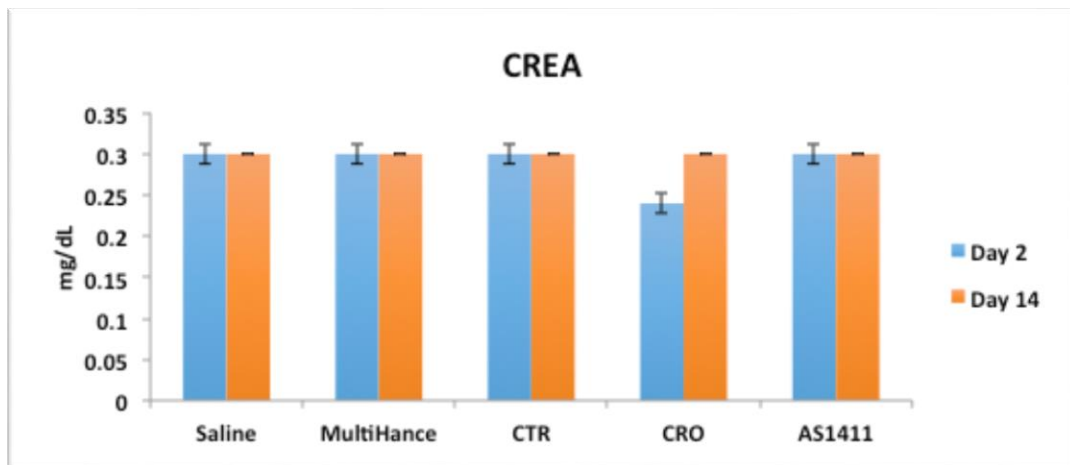


Figure 24: CREA post-treatment blood concentrations of 5 treatment groups

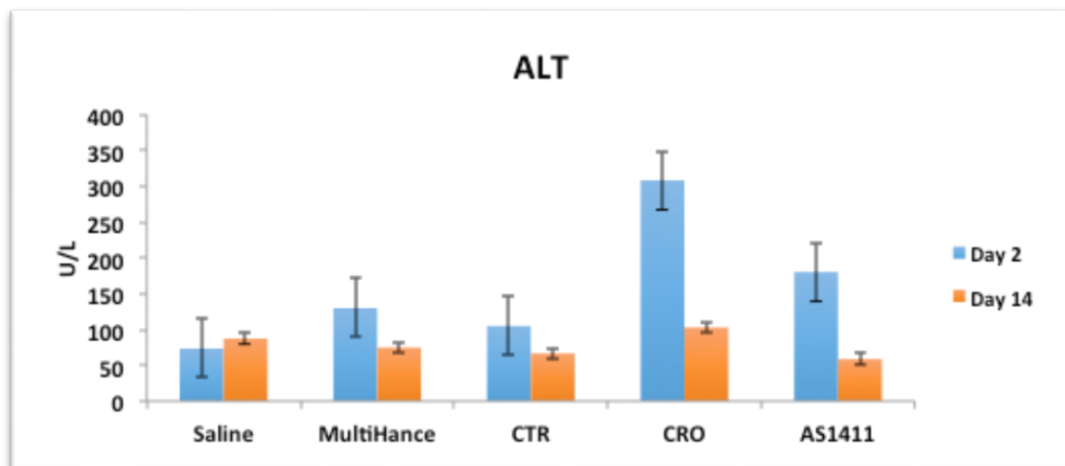


Figure 25: ALT post-treatment blood concentrations of 5 treatment groups.

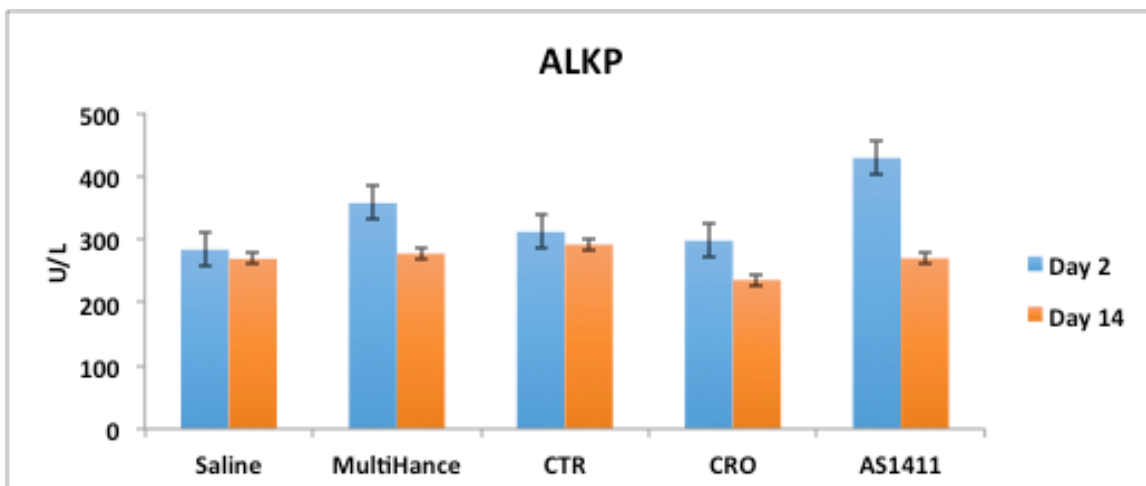


Figure 26: ALKP post-treatment blood concentrations of 5 treatment groups.

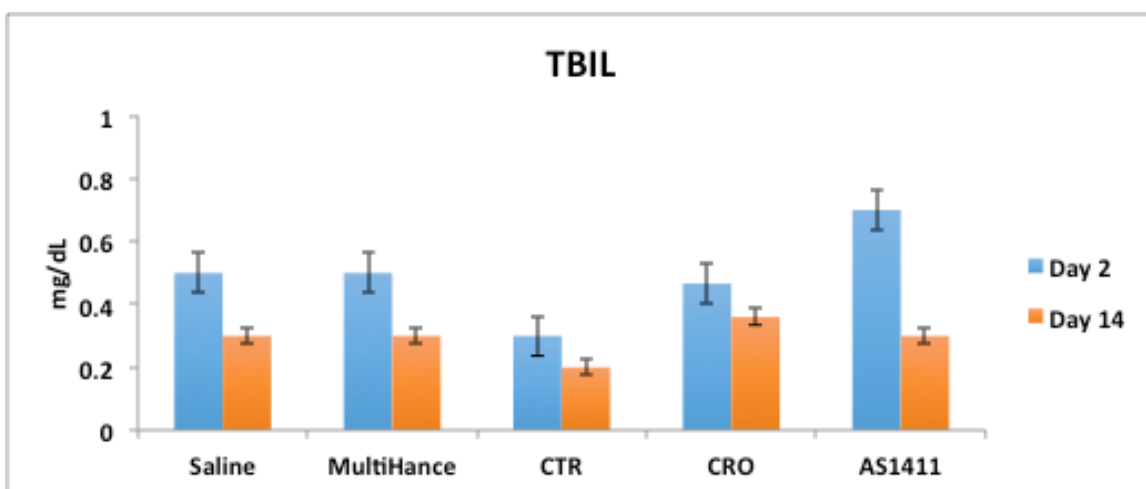


Figure 27: TBIL post-treatment blood concentrations of 5 treatment groups.

- To simplify the figures, CTR stands for GNP *Gd (III) DO3A-SH* CTR, CRO stands for GNP *Gd (III) DO3A-SH* CRO, and AS1411 stands for GNP *Gd (III) DO3A-SH* AS1411.

As demonstrated in figures 23-27 the post-treatment blood levels of BUN (mg/dL), CREA (mg/dL), ALT (U/L), ALKP (U/L), and TBIL (mg/dL) were plotted for the five different treatment groups at day 2 and day 14.

(c) Statistical Analysis:

We performed two statistical tests on the blood chemistry results to analyze the data that were collected. The first test is based on using unpaired t-tests by assuming all the involved biomarkers in this experiment are independent. The second statistical test is based on using ANOVA test in order to make a group analysis in case the collected biomarkers are dependent/correlated.

First, post-treatment blood biomarkers BUN, CREA, ALT, ALKP, and TBIL values were analyzed by using unpaired T test, Tables 8 and 9. The blood biomarkers for each group (MultiHance, GNP *Gd (III) DO3A-SH* CTR, GNP *Gd (III) DO3A-SH* CRO, GNP *Gd (III) DO3A-SH* AS1411) were compared with blood biomarkers for a saline control group at days 2 and 14 respectively. As demonstrated in Table 8, the statistical results show that all of the variables do not have a significant difference between GNP *Gd (III) DOA3-SH* AS1411 and control group at day 2. However, the unpaired t-test detects significant differences occur for BUN and CREA biomarkers for the following post-treatment agents: MultiHance, GNP *Gd (III) DOA3-CTR*, and *Gd (III) DOA3-CRO* as demonstrated by bold highlighted values in Table 8. In a similar way, Table 9 shows the estimated P-values by day 14. It is clear that there are no significant differences between biomarkers blood levels of the animals injected with test solution GNP *Gd(III)-DO3A-SH-AS1411* and biomarkers blood levels of the animals injected with saline solution.

Table 8: P-values of unpaired T test for day 2 post-treatment

Blood Biomarker	Saline & MultiHance	Saline & GNP <i>Gd (III) DO3A-SH</i> CTR	Saline & GNP <i>Gd (III) DO3A-SH</i> CRO	Saline & GNP <i>Gd (III) DO3A-SH</i> AS1411
BUN	0.0078	0.0085	0.0073	0.3322
CREA	1.000	1.000	0.0278	1.000
ALT	0.1605	0.1605	0.0795BUN, CREA	0.2196
ALKP	0.0565	0.0565	0.7108	0.0515
TBIL	1.000	1.000	0.8836	0.6305

Table 9: P-values of unpaired T test for day 14 post-treatment:

Blood Biomarker	Saline & MultiHance	Saline & GNP <i>Gd (III) DO3A-SH</i> CTR	Saline & GNP <i>Gd (III) DO3A-SH</i> CRO	Saline & GNP <i>Gd (III) DO3A-SH</i> AS1411
BUN	0.4482	0.9152	0.9256	0.2155
CREA	1.000	1.000	1.000	Perfect data
ALT	0.4253	0.1713	0.6656	0.0844
ALKP	0.8178	0.5414	0.3824	0.9619
TBIL	1.000	0.1525	0.6317	1.000

For more investigation, we performed an ANOVA test in case there are correlations between the measured biomarkers. In this statistical test, we used a factorial design with post-treatment interval (2 days or 14 days) and treatment agents, along with their interaction effect. The dependent variables were the log-transformed post-treatment biomarkers relative to control: in ($BUN_{Test} / BUN_{Control}$), etc. The linear model was fit to each biomarker independently. The ANOVA was performed to test whether there was any significant treatment agent-dependence on the change in biomarker levels. The results show that the BUN, ALT, ALKP, and TBIL data were not significantly different from our

null hypothesis that there is a significant treatment agent-dependence on the change in biomarker levels ($\chi^2 = 15.2, 12.3, 12.5, 9.45$ respectively, with 9 degrees of freedom [d.f.]; $p = 0.08, 0.20, 0.19, \text{ and } 0.051$ respectively).

Both statistical tests (unpaired t-tests and ANOVA) demonstrate that there are no significant difference in post-treatment blood levels of BUN, ALT, CREA, ALKP, and TBIL between GNP *Gd (III) DOA3-SH AS1411* and saline group, which means the proposed contrast agent (*Gd (III) DOA3-SH AS1411*) does not affect liver and kidney functions and it is safe for animals.

CHAPTER 4: CONCLUSIONS

We have developed cancer-targeted gold nanoparticle-based MRI contrast agent consisting of: a 4 nm diameter gold nanoparticle, cancer targeting DNA aptamer (AS1411), and a gadolinium chelate contrast agent (*Gd(III)-DO3A-SH*). The particles were characterized using DLS, UV-vis, and TEM. Zeta potential for GNP *Gd (III) DOA3-SH* AS1411 was -20.9 ± 1.1 which, displayed high stability. The selective targeting ability was evaluated by in-vitro study using MDA-MB-231 and MCF-10A cell lines. AS1411 is included in the coating to allow the nanoparticles to be selectively retained in cancer cells upon binding to nucleolin protein, which is expressed on the cell surface and in the cytoplasm of cancer cells. Since nucleolin is found solely in the nucleus of healthy cells, where it is unavailable for binding to our nanoparticles, AS1411-coated particles are not retained in healthy cells.

Oligonucleotide anchoring to the nanoparticle surface, along with steric crowding within the corona monolayer, slows the rotational tumbling rate of the Gd^{3+} chelate and therefore reduces the T1 relaxation time, hence increasing the T1-Weighted image contrast of GNP-*Gd(III)DO3A-SH*-Oligonucleotide. The local voxel wise and global image analysis of T1- Weighted algorithm on GNP-*Gd(III)DO3A-SH*-Oligonucleotide construct

has shown exceptional contrast enhancement for MDA-MD-231 cells targeted by the cancer specific contrast agent GNP-*Gd(III)DO3A-SH-AS1411* compared to its non-targeted control counterparts GNP-*Gd(III)-DO3A-SH-CRO/CTR*. The nucleolin binding ability of AS1411 oligonucleotide has led to selective accumulation of gadolinium-based contrast agent (GBCA) in cancer cells (MDA-MB-231) accomplishing superior contrast enhancement over non-malignant breast epithelial cells (MCF-10A). Moreover, the T1-Weighted image analysis algorithm features steric bulk-induced longitudinal changes by yielding significantly higher T1-Weighted image for GBCA with longer sequence oligonucleotides (AS1411/CRO) in comparison to their shorter sequence counterpart CTR, particularly in the breast cancer cells. All of these studies suggest that GNP-*Gd(III)DO3A-SH-AS1411* has the potential use of enabling discrimination between cancerous and healthy tissue using MRI.

Our in-vivo toxicity and biodistribution study shows that the proposed contrast agent GNP (*Gd(III)-DO3A-SH-AS1411*) is not toxic for healthy rats. ICP-MS analysis demonstrates that the particles were cleared from all body organs. Although there are elevated levels of GNP-*Gd(III)DO3A-SH-AS1411* in the liver and spleen, the concentrations of the particles on day 14 are less than the concentrations in day 2 for both organs, suggesting ongoing clearance of nanoparticles from these organs.

We selected five blood biomarkers to evaluate the toxicity of the contrast agent. BUN and CREA were used to evaluate kidney function and ALT, TBIL, and ALKP were used to evaluate liver function. Our statistical analysis results show that there is not any significant difference between biomarkers blood levels of the animals injected with test solution GNP *Gd(III)-DO3A-SH-AS1411* and biomarkers blood levels of the animals

injected with saline solution.

Our proposed cancer-targeted contrast agent (GNP (*Gd(III)*)-*DO3A-SH*-AS1411) exhibits MRI contrast with higher relaxivity in cancer cells in comparison to normal cells by in vitro study ,and the particles were not toxic for healthy animals. The evidence thus far suggests that GNP-*Gd(III)**DO3A-SH*-AS1411 is worth investigating further both in vitro and in vivo to optimize cancer targeting and contrast capabilities.

REFERENCES

1. Center for Disease Control and Prevention, 2015: <https://www.cdc.gov>.
2. American Cancer Society, 2018: <https://www.cancer.org/>.
3. OECD. 2015; Available from: <https://data.oecd.org/>.
4. D. W. McRobbie, E. A. Moore, M. J. Graves, and M. R. Prince, "MRI from Picture to Proton," *Cambridge University Press*, 2007, ISBN 1139457195.
5. Molecular Imaging and Contrast Database (MICAD). 2004-2013.
6. Morcos, S.K. and H.S. Thomsen, Adverse reactions to iodinated contrast media. *Eur Radiol*, 2001. 11(7): p. 1267-75.
7. Marckmann, P., et al., Nephrogenic systemic fibrosis: suspected causative role of gadodiamide used for contrast-enhanced magnetic resonance imaging. *J Am Soc Nephrol*, 2006. 17(9): p. 2359-62.
8. EM Reyes-Reyes, FR Šalipur, M. Shams, MK Forsthoefel, and PJ Bates, "Mechanistic studies of anticancer aptamer AS1411 reveal a novel role for nucleolin in regulating Rac1 activation," *Mol Oncol*. 2015 Aug;9 (7):1392-405.
9. MT Malik, MG O'Toole, LK Casson, SD Thomas, GT Bardi, EM Reyes-Reyes, CK. Ng, KA. Kang, and PJ. Bates," AS1411-conjugated gold nanospheres

- and their potential for breast cancer therapy,” *Oncotarget*. 2015 Sep 8; 6(26): 22270–22281.
10. R. Chauhan, N. ElBaz, K. T. James, D. A. Malik, M. Zhu, A. ElBaz, R. S. Keynton, C. K. Ng, P. J. Bates, T. Malik, M. G. O' Toole, “Targeted Contrast Agents for Imaging of Triple Negative Breast Cancer and Local Voxel-wise MRI Analysis Algorithm,” *Nano Research Journal*, Submitted.
 11. Z. Zhou and Z. Lu, “Gadolinium-Based Contrast Agents for MR Cancer Imaging,” *Wiley Interdiscip Rev Nanomed Nanobiotechnol*. 2013 Jan; 5(1): 1–18.
 12. Masitas, R. A.; Zamborini, F. P., Oxidation of Highly Unstable <4 nm Diameter Gold Nanoparticles 850 mV Negative of the Bulk Oxidation Potential. *Journal of the American Chemical Society*. 2012, 134 (11), 5014-5017.
 13. Lebduskova, P.; Hermann, P.; Helm, L.; Toth, E.; Kotek, J.; Binnemans, K.; Rudovsky, J.; Lukes, I.; Merbach, A. E., Gadolinium(iii) complexes of mono- and diethyl esters of monophosphonic acid analogue of DOTA as potential MRI contrast agents: solution structures and relaxometric studies. *Dalton Transactions*. 2007, (4), 493-501.
 14. Lacerda, S.; Campello, M. P.; Marques, F.; Gano, L.; Kubicek, V.; Fouskova, P.; Toth, E.; Santos, I., A novel tetraazamacrocyclic bearing a thiol pendant arm for labeling biomolecules with radiolanthanides. *Dalton Transactions*. 2009, (23), 4509-4518.
 15. Chang, T.-C.; Yu, S. J., Microwave-Assisted Catalytic Acetylation of Alcohols by Gold-Nanoparticle-Supported Gadolinium Complex. *Synthetic Communications*. 2015, 45 (5), 651-662.

16. Hurst, S. J.; Lytton-Jean, A. K. R.; Mirkin, C. A., Maximizing DNA Loading on a Range of Gold Nanoparticle Sizes. *Analytical Chemistry*. 2006, 78 (24), 8313-8318.
17. Warsi, M. F.; Chechik, V., Strategies for increasing relaxivity of gold nanoparticle based MRI contrast agents. *Physical Chemistry Chemical Physics*. 2011, 13 (20), 9812-9817
18. Barge, A.; Cravotto, G.; Gianolio, E.; Fedeli, F., How to determine free Gd and free ligand in solution of Gd chelates. A technical note. *Contrast media & molecular imaging*. 2006, 1 (5), 184-188.
19. Su, Y.; Tan, M. L.; Lim, C. W.; Teo, S. K.; Selvaraj, S. K.; Wan, M.; Zhong, L.; Tan, R. S. In Automatic correction of motion artifacts in 4D left ventricle model reconstructed from MRI, *Computing in Cardiology*. 2014, 7-10 Sept. 2014; 2014; pp 705-708.
20. W. Haiss, N. Thanh, J. Aveyard, D. Fernig; Determination of Size and Concentration of Gold Nanoparticles from UV-Vis Spectra. *Anal. Chem*. 2007, 79, 4215-4221
21. Integrated DNA Technologies: <http://www.idtdna.com/pages>.

CURRICULUM VITAE

Nagwa El-Baz

Research Assistant, Department of Pharmacology & Toxicology

University of Louisville

n0elba01@louisville.edu

Education

- | | |
|--------------|---|
| 2017-Present | Ph.D. student in Pharmacology and Toxicology, University of Louisville, USA |
| 2015-Present | M.S. student in Pharmacology and Toxicology, University of Louisville, USA |
| 1996-2001 | B.S. in Pharmacy, Mansoura University, Egypt |

Professional Experience

- | | |
|--------------|--|
| 2015-Present | Research Assistant, O'toole's Laboratory, Bioengineering Department, University of Louisville, USA |
| 2001-2002 | Phamacist, Elsinblaween Hospital, Egypt |

Publications

1. N. El-Baz, D. Malik¹, R. Chauhan, K. James, M. Zhu, J. Li, A. El-Baz, D. Miller, R. Keynton, C. Ng, P. Bates, M. Tariq Malik, M. O' Toole, "Targeted Theranostic Gold Nanoparticles for Imaging and Therapy of Triple Negative Breast Cancer," Biomedical Engineering Society (BMES), October 5-8, 2016 in Minneapolis.
2. D. Malik*, N. ElBaz*, R. Chauhan*, K. James, M. Zhu, J. Li, A. ElBaz, D. Miller, R. Keynton, C. Ng, P. Bates, , M. O' Toole, M. Malik, "Nanotheranostic: Targeted Aptamer Nanoparticles for Breast Cancer Therapy and Imaging," Boston, USA, June 2016. Note that '*' means co-first author.
3. M. Malik, M. O'Toole, D. Malik, R. Chauhan, M. Zhu, C. Ng, J. Li, H. Zheng, K. James, N. El-Baz, N. Bilcuhuk, A. El-Baz, R. Keynton, A. Dragun, B. Wang, N. Dunlap, D. Miller and P. Bates, "AS1411-GNS: A Platform Technology for Cancer-targeted Therapy and Imaging," Imaging 2020: The Future of Precision Medicine Molecular Imaging for Diagnosis and Surgery/Therapy, Jackson Lake Lodge, Moran, Teton County, Wyoming, September, 2016.
4. N. El-Baz, R. Chauhan, K. T. James, D. A. Malik, M. Zhu, Junling Li, A. El-Baz, D. M. Miller, R. S. Keynton, C. K. Ng, P. J. Bates, T. Malik, M. G. O' Toole, "A Novel Image Monitoring Algorithm For Triple Negative Breast Cancer," Biomedical Engineering Society (BMES), October 2017 in Phoenix, USA.
5. N. El-Baz, K. James, R. Chauhan, D. Malik, B. Nunn, A. Switala, A. El-Baz, R. Keynton, P. Bates, T. Malik, M. O'Toole, " In Vivo Assessment of Toxicity of Gold Nanotheranostic Agent", April 2018 in Atlanta, USA.

Seminar and Oral Presentations

1. N. El-Baz, "Cancer Targeting MRI Contrast Agent," Pharmacology and Toxicology Department Research Seminar, March 2016.
2. N. El-Baz, "Cancer Targeting MRI Contrast Agent," JGBCC Seminar Series, May 2016.